NACA RM E50E03

[redacted]

cy 2

NACA

RESEARCH MEMORANDUM

INVESTIGATION OF AERODYNAMIC AND ICING CHARACTERISTICS OF WATER-INERTIA-SEPARATION INLETS FOR TURBOJET ENGINES

By Uwe von Glahn and Robert E. Blatz

Lewis Flight Propulsion Laboratory
Cleveland, Ohio

NATIONAL ADVISORY COMMITTEE
FOR AERONAUTICS

WASHINGTON
July 26, 1950

NACA RM E50E03

NATIONAL ADVISORY COMMITTEE FOR AERONAUTICS

RESEARCH MEMORANDUM

INVESTIGATION OF AERODYNAMIC AND ICING CHARACTERISTICS OF WATER-INERTIA-SEPARATION INLETS FOR TURBOJET ENGINES

By Uwe von Glahn and Robert E. Blatz

SUMMARY

The results of an investigation of several internal water-inertia-separation inlets consisting of a main duct and an alternate duct designed to prevent automatically the entrance of large quantities of water into a turbojet engine in icing conditions are presented. Total-pressure losses and icing characteristics for a direct-ram inlet and the inertia-separation inlets are compared at similar aerodynamic and simulated icing conditions.

Complete ice protection for inlet guide vanes could not be achieved with the inertia-separation inlets investigated. Approximately 8 percent of the volume of water entering the nacelles remained in the air passing into the compressor inlet. Heavy alternate-duct-elbow ice formations caused by secondary inertia separation resulted in rapid total-pressure losses and decreases in mass flow. The duration in an icing condition for an inertia-separation inlet, without local surface heating, was increased approximately four times above that for a direct-ram inlet with a compressor-inlet screen. For normal nonicing operation, the inertia-separation-inlet total-pressure losses were comparable to a direct-ram installation. The pressure losses and the circumferential uniformity of the mass flow in all the inlets were relatively independent of angle of attack. Use of an inertia-separation inlet would in most cases require a larger diameter nacelle than a direct-ram inlet in order to obtain an alternate duct sufficiently large to pass the required engine air flow at duct Mach numbers below 1.0 at the minimum area.

INTRODUCTION

Turbojet-engine ice protec :on by means of an inlet designed to separate the free liquid water from the intake air by water

inertia separation is shown to have possibilities in reference 1. All the inlets investigated consisted of a single-inlet nacelle (fig. 1) followed by a main duct for nonicing operation and an alternate duct with sharply curved passages through which air, with a reduced water content, passed to the compressor unit during an icing condition. The results obtained in the investigations of reference 1 showed that complete water separation could be obtained only at the expense of considerable total-pressure losses when the air passed through the alternate duct. The water-separation effectiveness of inertia-separation inlets is shown in reference 1 to be a function of alternate-duct-inlet gap (fig. 1), radial offset of the duct-splitter ring with respect to the nacelle inlet, curvature of the alternate-duct surfaces, and air velocity through the duct. Design charts in reference 1 indicate that small inlet gaps are required to prevent small cloud droplets from entering the alternate duct. A small inlet gap, however, limits the mass flow through the alternate duct and produces high duct-air velocities that cause large pressure losses.

Several improved designs, based on the investigation of reference 1, were developed at the NACA Lewis laboratory; these designs were intended to operate in nonicing conditions at pressure-loss values comparable to direct-ram inlets and to give adequate ice protection with satisfactory pressure recovery through the alternate duct in an icing condition.

The four water-inertia-separation inlets evaluated herein were designed with the aid of a simplified analysis and the design charts presented in reference 1, whereas the inlets previously investigated were designed by a systematic variation of the configuration components prior to the development of design charts. Aerodynamic and icing studies of these four water-inertia-separation inlets reported herein were conducted in the NACA 6- by 9-foot icing-research tunnel. The data were analyzed to obtain pressure-loss values at similar mass air flows and to compare the icing tolerance that can be obtained with inertia-separation inlets with that obtained with a conventional direct-ram inlet.

SYMBOLS

The following symbols are used in this report:

A area, square feet

h' radial offset of duct-splitter ring, inches

L height of duct at instrumentation stations, inches

l distance from outer duct wall to pressure-measuring tube, inches

M Mach number

m mass flow, pounds per second

m/m_1 ratio of mass flow after time interval to initial mass flow

P total pressure, pounds per square foot

R alternate-duct-inlet turning radius, inches

V indicated airspeed, miles per hour

α angle of attack of nacelle, degrees

Subscripts:

0 free stream

2 compressor inlet

a alternate duct

av average

i initial condition

APPARATUS AND INSTRUMENTATION

The inlets investigated (See fig. 2 for typical model.) were constructed of wood and had a 28-inch maximum diameter. At the vertical plane of the inlet guide vanes or compressor inlet, the internal duct had a 19.3-inch outside diameter and a 13.3-inch inside diameter (accessory-housing diameter), which resulted in a compressor-inlet area of approximately 155 square inches for all inlets investigated. The various configurations were designed to provide two concentric annular ducts separated by a duct-splitter ring. The principal components of a typical internal water-inertia-separation inlet are shown in figure 1. The nose inlets were mounted on the circular afterbody used in the investigation reported in reference 2.

The angle of attack of the model was varied by turning the model in a horizontal plane. The top and the bottom of the nacelle thus corresponded to the horizontal axis of a typical nacelle on an aircraft.

Two types of main-duct compressor-inlet screen were used in the investigation. The purpose of these screens was to obtain rapid blockage of the main duct in an icing condition and cause the water inertia separation provided by the alternate duct to become effective before the guide vanes iced severely. The first screen consisted of concentric streamlined wires 0.192 inch in chord and 0.048 inch in thickness with a center-line spacing of 0.312 inch. The second screen, used as a substitute for the first screen, consisted of concentric round wires of 0.062-inch diameter with a center-line spacing of 0.156 inch. No screen was installed in the alternate duct.

A group of four flat blades (fig. 1), each 0.75 by 3.0 inches in size, 0.062 inch thick, and spaced 90° apart circumferentially at the compressor-inlet section, served as ice indicators. The blades were mounted with the 0.75-inch dimension parallel to the air stream. The size of these blades was such that a high water-collection efficiency was assured and a comparison of the quantity of ice collected on the blades for the various inlets in icing conditions was an indication of the inertia-separation effectiveness. For some studies, one of the flat blades was replaced by a typical 1-inch-chord curved inlet guide vane in order to determine its icing characteristics in an inertia-separation inlet. In order to determine the icing characteristics in the alternate duct, an ice-indicator rod of 0.062-inch diameter was placed in the vertical plane of the trailing edge of the duct-splitter ring (fig. 1).

At the compressor-inlet plane, four 9-tube electrically heated rakes were used to determine the radial profiles of velocity, mass flow, and total pressure. The center tube in each rake was a static-pressure tube and the remainder were total-pressure tubes. The rakes were circumferentially spaced about the compressor inlet in order to determine the aerodynamic effects of angle of attack on the performance of the various inlets. Two additional rakes, each consisting of five heated tubes (four total-pressure tubes and a static-pressure tube), were mounted in the alternate duct (fig. 1) on the horizontal axis of the model center line. Two electrically heated static-pressure tubes were mounted in the main duct ahead of the screen between the duct-splitter ring and the accessory housing. Pressure readings from all the rakes were photographically recorded from multiple-tube manometers.

CONFIGURATIONS

Four inertia-separation inlets and one direct-ram inlet were investigated. Coordinates for all inlets with reference to the nacelle nose in the direction of the x-axis and the nacelle center line in the direction of the y-axis are given in tables I to III. The outer contours and the inlet-lip radii were designed on the basis of results reported in reference 1.

The following table presents the principal design dimensions and area ratios for the alternate ducts of the inlets investigated:

Configuration	Minimum nacelle-inlet area (sq in.)	Radial offset h' (in.)	Design inlet gap (in.)	Design minimum area at inlet gap (sq in.)
A	109	---	---	--
B	109	2.2	1.3	71
C	154	1.5	1.6	85
D	154	1.4	1.4	74
E	154	1.1	1.9	99

During fitting of the various components and installation in the tunnel, small changes in the dimensions were unavoidable and the effects of these changes will be subsequently discussed.

Cross sections of the inlets investigated are shown in figure 3. For configurations A and B, the inlets were designed to accommodate a standard production turbojet engine; whereas for configurations C, D, and E the entrance leading to the compressor was modified in the interests of improved air flow by a sheet-metal fairing, as shown in figure 1.

The internal contours of the direct-ram inlet (configuration A) served as a base line for the design of an alternate duct. The alternate-duct inlet was chosen to be near the accessory-housing nose (fig. 1) in order that the radial offset of the duct-splitter-ring nose did not cause an abrupt change in the main-duct area, with attendant large pressure losses. The alternate-duct gap was then calculated using the simplified design charts of reference 1 for a droplet size of 15 microns and a duct-air velocity at the gap of 550 miles per hour. The point at which the gap occurs in the alternate duct was arbitrarily chosen to occur at the 90° point of the turning radius (component G, fig. 1). The minimum area of the alternate duct was thus established at the alternate-duct gap.

This minimum area specifies the maximum mass flow that the alternate duct may pass. The area gradually increased downstream of the entrance of the compressor face. The angle that the main-duct screen makes with the accessory housing is determined by the space available between the trailing edge of the duct-splitter ring and the bearing struts or the guide-vane location. Configuration D was similar to C except that the gap of D was arbitrarily decreased 12 percent, as shown in figure 3. Configuration E resulted from the combination of the nacelle shell of configurations C and D with the duct-splitter ring of configuration B. The alternate-duct gap was set at 1.9 inches to pass a large mass flow, to reduce pressure losses, and to determine the water-separation effectiveness of large gap inlets.

PROCEDURE

The aerodynamic investigations were conducted in the Lewis 6- by 9-foot icing-research tunnel at a tunnel-air velocity of approximately 250 miles per hour. These investigations were made with the screens removed at angles of attack of 0°, 2°, 4°, and 6° to obtain aerodynamic data independent of screen losses, at mass flows per unit area ranging from 10 to 30 pounds per second per square foot. The model was also investigated for the same range of conditions with air flowing through only the alternate duct. The main duct was blocked with a plate at the screen location in order to simulate a fully iced screen.

The icing investigations for each configuration were conducted under similar tunnel icing conditions in order to provide a common basis for comparison. Each inlet was investigated at two different mass flows with the main duct blocked in order to determine the effect of air velocity through the alternate duct on the duct icing characteristics. The inlets were then investigated in icing conditions with the main-duct screen installed.

The icing studies were conducted at tunnel air velocities ranging from 100 to 250 miles per hour and at an angle of attack of 0°. Droplet size and water concentration were determined by rotating multicylinders. The mean effective droplet size was approximately 10 microns. Water concentrations from 0.6 to 1.5 grams per cubic meter were used. The total air temperature in the tunnel ranged from 10° to 20° F. The duration of the icing periods varied from 2 to 24 minutes. At the end of each icing period, photographs were taken of the nacelle nose and duct-splitter ring, the alternate duct and elbow, the compressor-inlet screen, and the various ice indicators.

RESULTS AND DISCUSSION

Aerodynamic Results

The pressure loss at various rake stations was calculated as P_0-P, where the total pressure P was obtained at the required instrumented station. The integrated average total-pressure loss of all the compressor-inlet-station rakes was chosen as the configuration pressure-recovery value. The results presented were not corrected for tunnel-wall interference and blocking effects. The total-pressure loss of the direct-ram inlet is used as a basis for comparison with the inertia-separation configurations investigated. The pressure loss of the various configurations is presented in terms of the mass flow per unit area measured at the compressor inlet. The effect of varying the angle of attack of the model from 0° to 6° on total-pressure loss, circumferential mass-flow variations, and velocity profiles at the compressor inlet were negligible for all inlets investigated; therefore all aerodynamic data are presented for an angle of attack of 0°.

Main-duct pressure losses. - In general, for normal nonicing operation, compressor air passed through only the main duct and the total-pressure loss for the configurations was a function of the nacelle-inlet area, the mass flow, and the area diffusion characteristics of the inlets. Only for very low mass flows did the air pass through the main and alternate ducts simultaneously for a nonicing condition; however, any effect due to flow in both ducts on the losses was negligible. The pressure loss in figure 4 is presented in terms of $(P_0-P_2)/P_0$. As shown in figure 4, the inlets having a large nacelle-inlet area (configurations C, D, and E) had a considerably lower pressure loss than the smaller nacelle-inlet-area configuration B because of the difference in dynamic pressure for similar mass flows. On a comparative basis, configurations C and D approach the pressure-loss values experienced with the direct-ram inlet (configuration A). Small changes in area at the alternate-duct inlet did not appreciably affect the main-duct pressure-loss values, as shown by a comparison of configurations C and D. The decrease in pressure-loss values for configuration E, as compared with values for configuration B, can be mainly attributed to the decreased dynamic pressure in the nacelle inlet, which resulted in lower expansion losses at the alternate-duct inlet. In addition, the improved design of the expansion section downstream of the duct-splitter ring (fig. 3) also contributed to a reduction in pressure losses.

From an analysis of the static-pressure measurements obtained in the region between the duct-splitter ring and the accessory housing, it was concluded that the flow separation off the duct-splitter ring occurred at the alternate-duct inlet, especially for configuration B. The smaller degree of flow separation for configurations C and D were due to the lower duct-velocity pressure for a given mass flow and to an improved fairing of the duct-splitter-ring leading edge. Configuration E showed a high degree of flow separation, similar to configuration B, primarily because the same duct-splitter ring was used. On the basis of the results obtained in these investigations, it appears feasible to expect a decrease in the pressure losses for configuration E by refairing the inner side of the duct-splitter ring so that a contour and area ratio similar to configurations C and D are obtained.

Alternate-duct pressure losses. - Pressure measurements made in the alternate duct with the main duct blocked by a closure plate to simulate complete blockage of the screen by ice (fig. 5) showed that, for low mass flows through the alternate duct, only a small loss in total-pressure ratio P_0-P_a/P_0 was experienced. At higher mass flows and as the choked air-flow condition for the ducts was approached, the pressure loss increased rapidly.

An analysis of the maximum mass flow passing through the various configurations indicates that configuration B operated at a mass flow greater than that produced by sonic velocity at the design minimum area. This condition could not exist, however, because the pressure differences available across the model were insufficient to induce sonic flow. It therefore is evident that the experimental alternate-duct-inlet gaps and areas may have varied from the design areas and gaps. The following table presents the mass flow at the choking Mach number based on the design values of the alternate-duct-inlet area for each inertia-separation inlet, the maximum air-flow values measured in the investigation, and the minimum design area of the alternate-duct inlet. It should be noted that the mass flow per unit flow area for most current turbojet engines is of the order of 30 pounds per second per square foot, or greater.

Configuration	Calculated mass flow at choking Mach number (design area) (lb/sec)	Maximum air flow (measured) (lb/sec)	Design area (sq in.)
B	22.2	23.6	71
C	26.6	22.0	85
D	22.6	21.5	74
E	31.0	23.7	99

A small change in the alternate-duct-inlet area or gap, or a small change in the location of the minimum-area point in the alternate duct, would change the Mach number considerably at large mass flows. Because of the complex curvatures of the configuration ducts, no accurate measurements of inlet areas could be obtained.

Extrapolation of the data presented in figure 5 for configuration B to a point at which the total-pressure-loss curve becomes approximately vertical (condition of choked air flow) indicates that the experimental minimum alternate-duct-inlet area must have approached a value of approximately 75 square inches rather than the design value of 71 square inches. Similar calculations for the remaining configurations indicate that the design areas were closely similar to the calculated experimental areas of the alternate-duct inlet. In view of these considerations, all calculations of Mach number in the following sections of this report in which configuration B is discussed were made using a minimum alternate-duct-inlet area of 75 square inches.

An analysis of the alternate-duct flow characteristics is shown in figure 6 where the Mach number at the minimum area of the alternate-duct inlet is presented as a function of the mass flow per unit area. If these curves are extended to the point where the duct Mach number is equal to unity, only configuration E would pass a mass flow comparable to current engines. At this mass flow, however, the attendant over-all total-pressure loss is extremely severe and unsatisfactory.

The over-all total-pressure-loss values at the compressor inlet for the inertia-separation models herein reported were very similar over the range of mass-flow values investigated (fig. 7). The high pressure losses shown in figure 7 were caused by losses in the alternate duct and the diffuser losses from the trailing edge of the duct-splitter ring to the compressor inlet. A plot of

the Mach number at the alternate-duct inlet as a function of overall total-pressure loss in the alternate duct indicates that the pressure losses at a given Mach number vary directly with the inlet gap (fig. 8). It is apparent that as small a gap as possible should be used in order to minimize the pressure losses at a specific Mach number, provided the required mass flow can be passed through the duct.

The curves shown in figures 6 and 7 may not necessarily be used for other values of free-stream Mach number M_0. Because of tunnel-airspeed limitations, it was impossible to differentiate satisfactorily the effects of small local configuration changes on pressure losses in the alternate duct from those effects that might be caused by the nacelle inlet at higher free-stream Mach numbers.

Calculations based on the experimental data showed that the diffuser efficiencies of the configurations from the trailing edge of the duct-splitter ring to the compressor-inlet section ranged from 60 to 77 percent.

The low diffuser-efficiency values obtained in the investigations are attributed to two factors: (1) the large effective angle of diffusion that was required in order to diffuse to the compressor inlet in a relatively short axial distance; and (2) the manner in which the closure plate, which blocked the main duct, fitted to the duct-splitter ring. Proper design of the diffuser section and the slope of the screen ahead of the compressor-inlet section might, on the basis of reference 3, give diffuser efficiencies in the order of 88 to 90 percent even at duct Mach numbers approaching 0.9. The correct screen slope is important because the screen, when iced, forms one wall of the diffuser (fig. 1).

Application of configurations investigated to existing engines. - As a basis for comparison with existing turbojet engines, the choking alternate-duct mass flows based on the design alternate-duct minimum areas are presented in the following table in terms of compressor-inlet flow area and projected compressor-inlet frontal area.

Configuration	Choking mass flow	
	Compressor-inlet flow area (lb/(sec)(sq ft))	Compressor-inlet frontal area (lb/(sec)(sq ft))
B	20.6	10.9
C	25.0	13.2
D	21.4	11.3
E	29.0	15.3

These data were calculated on the basis of a total pressure of 29.6 inches mercury and a total temperature of approximately 70° F. A mass-flow analysis of the configurations investigated shows that only the alternate duct of configuration E, if applied to a turbojet engine, would allow maximum engine air flow at rated engine speed; however, this air flow could only be passed through the duct at the choking Mach number with prohibitively high pressure losses. For full-scale considerations, the alternate-duct area must therefore be increased to an extent that it would pass sufficient air to the engine at a reasonable Mach number and pressure loss. This design requirement could be attained with configuration E by increasing the inlet gap about 26 percent and then scaling the entire configuration to fit the engine. An increase in the inlet gap, however, does not appear to be feasible for good water separation.

Sample calculations based on a corrected simplified analysis presented in reference 1 indicate that the configurations investigated greatly reduced the water that would otherwise be taken into an engine by a direct-ram inlet. The following table presents the results obtained from these calculations:

Droplet-size distribution (reference 4)	Droplet size (microns)	Free-stream airspeed (mph)	Ratio of water taken into engine with inertia-separation inlets to direct-ram inlet (percent)	
			Inlet B	Inlet E
A	5.0	250	15.6	28.6
A	7.5	250	2.0	16.4
A	10.0	250	0	3.0
A	12.5	250	0	0
E	10, mean effective	250	2.0	8.4

The assumptions made for these calculations were: (1) The simplified analysis of reference 1 is applied; (2) the flow is incompressible and at standard sea-level conditions with no nacelle-scooping effects; and (3) the maximum alternate-duct Mach number was assumed to be 0.6. Increasing the inlet gap for configuration E by 26 percent, as previously discussed, would permit a water intake of 18 percent of the water available at the nacelle inlet for the E droplet-size distribution in the preceding table.

Because the air velocity in the duct and the inlet gap are primary factors in determining the separation effectiveness of an inlet, the most feasible alternative in applying configuration E to an engine such as described in reference 1 would be to increase the radial location of the alternate-duct inlet from the center line of the nacelle, thereby increasing the inlet area of the alternate duct while maintaining the original gap dimension. This procedure would in most cases necessitate an increase in the over-all dimensions of a given nacelle installation, thereby increasing the drag of the nacelle, but maintaining good water-separation effectiveness.

Effect of total-pressure loss on thrust. - On the basis of studies reported in reference 5, the effect of a decrease in total pressure in an inlet causes a decrease in the thrust obtainable with an engine and also increases the specific fuel consumption. The relation of the total-pressure-loss ratio with thrust and specific fuel consumption is approximately linear and varies somewhat with free-stream Mach number. The loss in thrust is a function of the ram pressure loss as well as the loss in mass flow.

The loss in thrust and increase in specific fuel consumption to be expected with use of the inertia-separation inlets investigated herein are shown in figure 9 as a function of the Mach number at the alternate-duct inlet. The dashed lines indicate lines of constant mass flow. From the curves shown in figure 9, it is apparent that large performance losses can be anticipated for the inlets investigated herein for conditions of large mass flow and high alternate-duct Mach numbers. For an aircraft, this loss in thrust would occur when an icing condition was encountered that would cause the mass flow to shift to the alternate duct. Furthermore, the aircraft would continue at this reduced thrust even after passing out of the icing condition until the ice on the main-duct screen had been melted by operation in warmer ambient air. Operation of an engine at reduced thrust and increased fuel consumption for any great length of time would considerably reduce the speed and range of an aircraft.

Velocity distribution at compressor inlet. - Typical radial profiles of velocity (fig. 10) are shown plotted in terms of the ratio of the local velocity to the average velocity at a given rake station as a function of duct width ratio l/L. All data for the normal nonicing operating condition (fig. 10(a)) were obtained without screens in the duct and at maximum air flow. All inlets investigated showed a pronounced tendency for the flow to separate off the inner surface of the duct-splitter ring, confirming an

analysis of the static-pressure readings obtained in the region between the duct-splitter ring and accessory housing, from which it was concluded that flow separation occurred near the leading edge of the duct-splitter ring. The percentage variation of the radial profiles of velocity was approximately ±10 percent of the average velocity at the compressor face.

Radial profiles of velocity obtained in the alternate duct with the main duct blocked at maximum air flows (fig. 10(b)) indicate that for a narrow alternate-duct gap (configuration B) the air flow tends to separate from the outer surface of the duct-splitter ring. For large alternate-duct gaps (configuration E), the flow tends to separate in the elbow at the nacelle-wall surface. The nonuniform profiles of velocity at the compressor inlet with the main duct blocked (fig. 10(c)) indicate air-flow separation at the end of the duct-splitter ring. The percentage variation of the velocity across the duct at the compressor inlet averaged approximately ±20 percent. No appreciable changes were observed in the profiles with a change in mass flow.

The effects of a nonuniform velocity at the compressor inlet on compressor performance have not been evaluated; hence, no estimate can be made at this time of the loss in thrust that could occur by use of such nonuniform velocity profiles.

Icing Characteristics

The icing characteristics for the configurations investigated were similar, differing only as to extent and local quantity of ice on the various engine components. Because of this similarity of icing characteristics, generalized descriptions of component icing are presented with minor differences pointed out as required. The icing photographs presented herein are typical for all inlets except where stated. The solid lines of the sketches included with some of the photographs indicate the configuration components that are seen in the icing photograph.

Typical ice formations on the nacelle-inlet lips and accessory housing, as shown in figures 11(a) and 11(c), were very similar to those encountered in natural icing conditions (reference 6). The icing of the nacelle-inlet walls was dependent on the inlet-velocity ratios. In all cases, wall ice formations were observed at low mass-flow values that corresponded to low inlet-velocity ratios (fig. 11(b)), whereas for high mass-flow values or high inlet-velocity ratios no such wall ice formations were observed (fig. 11(c)).

The effect of icing on the remainder of the nacelle components will be discussed in detail because the manner in which they tended to ice indicated the effectiveness of the inertia-separation inlets.

Screen icing. - In general, the icing of the round-wire screen was similar for all configurations (fig. 12(a)). As the round wires began to ice, the ice formations were parallel to the air stream; however, as the effective frontal area was reduced by the ice, the air curved around these formations and passed through the staggered rows of wires, in turn causing the ice formations to curve toward the accessory housing. Total pressure and aerodynamic forces on the ice formation sometimes became too great and the ice ridges broke off and were passed through or lodged against the screen, causing rapid and severe momentary mass-flow and total-pressure fluctuations. This rupture of the ice ridges occurred with both rime and glaze ice.

When the streamlined-wire screen with the greater wire spacing was used, the curving of the ice formations as a result of the stagger of the screen wires was even more evident. The greater collection efficiency of the streamlined wires caused a more rapid buildup of ice than the round wires. A mushrooming tendency of the ice formations on the streamlined-wire screen is shown in figure 12(b).

Duct-splitter ring. - The ice formations on the leading edge of the duct-splitter rings (fig. 13) for the configurations investigated extended into the alternate duct to a point at which the surface of the ring was tangent to the leading-edge radius of the ring. For cases when the ice formations on the leading edge also extended into the main duct, the ice tended to project forward into the air stream along the portions that were protruding into the main duct and in time might have blocked the alternate-duct inlet.

Alternate duct. - The ice formations in the alternate-duct elbow were caused by secondary inertia separation in the turn from the alternate-duct inlet to the alternate duct formed by the duct-splitter ring and the nacelle wall. Because of this effective secondary separation, however, the ridges of ice in the alternate-duct elbow built up very rapidly and choked the elbow to such an extent that the mass flow and total-pressure losses were severely affected.

Front and rear views of a typical ice ridge in the elbow of configuration E are shown in figures 14(a) and 14(b), respectively. These ice ridges occurred approximately halfway through the elbow and protruded into the air stream, thereby reducing the effective duct area. At times, the ridges were very thin and broke off unevenly during an icing period, which caused severe fluctuations and shifts in mass flow and total-pressure losses.

Because secondary inertia separation occurs in the alternate-duct elbow, a considerable amount of the remaining water in the incoming air is concentrated near the alternate-duct nacelle wall, as shown by the ice formation on the 0.062-inch-diameter ice-indicating rod in figure 15. The profile of the ice formation shown in figure 15 was turned approximately 90° to the air flow to facilitate photographing the ice formations.

Bearing struts. - Comparative photographs of bearing-strut icing for a direct-ram inlet (no screen) and water-inertia-separation inlets are shown in figure 16. Bearing-strut icing is a minor factor with water-inertia-separation inlets (fig. 16(b)), whereas with a direct-ram inlet extremely severe icing occurs (fig. 16(a)). The heavy deposits of ice near the nacelle walls of the struts for the direct-ram inlet were caused by the deflection characteristics of the accessory housing and the ice formations on the nose of this housing.

Inlet guide vanes. - With the direct-ram inlet (no screen), extremely severe ice formations on the indicator blades were observed (fig. 17(a)). The straight blades had as much as 2 inches of ice on the leading edge with a maximum frontal thickness of almost 1 inch during an icing period of 15 minutes.

Straight-indicator-blade icing characteristics are shown in figure 17(b) for a typical inertia-separation inlet. The greatest amount of ice with any configuration was approximately 0.25 inch for an icing period of 20 minutes. For most inlets, the over-all separation effectiveness was substantially similar and the differences in separation qualities were of a local nature. An examination of the magnitude of ice formations collected on the straight flat blades for configuration A (with no screen, fig. 17(a)) and configuration E (fig. 17(b)) shows that the water collection in the form of ice for the configuration E blade is approximately 8 percent of that for the direct-ram inlet. This quantity of water collection is in close agreement with calculated water-volume-intake percentage (8.4 percent) previously discussed.

The curved blade for configuration A (fig. 18(a)) was subjected to the same icing condition as the flat blade in figure 17(a).

The concave side of the curved blade was heavily iced and, based on the conventional close spacing for this size blade in an engine, the inlet guide vanes would have been completely blocked except near the accessory-housing surface.

Typical curved-indicator-blade icing for inertia-separation inlets is shown in figure 18(b). Under no conditions were large deposits of ice observed on the curved blade when the inertia-separation inlets were used for icing periods up to 20 minutes, and furthermore, no noticeable mushrooming of the ice occurred at the leading edge.

Aerodynamic Effects of Icing

Although an engine would not experience a decrease in mass flow in the same measure as the inlets investigated, the reduction in the mass flow through the inlets in an icing condition is indicative of the rate of ice formation and pressure loss in the various duct passages. Aerodynamic data for the icing investigations conducted with the configurations are therefore presented in terms of the mass-flow ratio m/m_1 as a function of time in an icing condition. Investigations were made to determine the total-pressure loss and the decrease in mass flow with time under varying icing conditions, free-stream velocities, mass flows, and type of main-duct screen.

The general effect of some of these variables for configuration A is presented in figure 19. For similar icing conditions, the mass-flow rate was reduced more rapidly at high initial mass flows than at low initial mass flows. The increased curvature of the flow field ahead of the nacelle for conditions of low nacelle air flow decreased the total amount of liquid water taken into the nacelle inlet for these particular investigations. The reduction of water in the nacelle main duct decreased the icing rate of the screen and consequently the mass-flow reduction rate is also decreased. By a similar procedure, the icing rate for the inertia-separation inlets is decreased at low mass-flow rates.

In general, the effect of the type of ice, glaze or rime, is that glaze ice, which prevails at higher air temperatures, caused a more rapid blocking of the screen and consequently a decrease in the time required to reach a given mass-flow value than did rime ice, as indicated in figure 19.

The effect of the type of ice on mass-flow reduction was not observed in the inertia-separation configurations because of the

flow shift from the main duct into the alternate duct. The resulting ice formation in the alternate-duct elbow controlled the reduction in mass flow, and the ice formations were of such a nature as to produce approximately similar mass-flow reduction rates in all the configurations. Comparisons of the reduction of mass flow through the inertia-separation configurations as a function of time in an icing condition at two ambient-air temperatures are shown in figure 20. This figure shows that, by the use of water-inertia-separation inlets, the time required to reach a given percentage of mass-flow decrease is approximately four times greater than that required by a direct-ram inlet (with screen) to reach the same value of mass flow.

The loss in total pressure with time in an icing condition gave the same general results as discussed for the mass flow. In general, the time required for the total-pressure loss to reach a particular value for the inertia-separation inlets was approximately four times greater than that required for the direct-ram inlet. Icing investigations of the direct-ram inlet without a screen showed an approximate loss of 1.5 percent of the initial total-pressure value during an icing period of 15 minutes and for maximum air flow through the model.

CONCLUDING REMARKS

All surfaces of a turbojet-engine inlet on which heavy icing occurs must be heated to prevent excessive ice buildup that may impair the aerodynamic performance. These surfaces include the nacelle-inlet lips, duct-splitter-ring leading edge, alternate-duct elbow and nacelle-wall surface, and the nose of the accessory housing. The icing of the accessory housing may be serious only for icing conditions in which glaze ice is encountered or rime-icing periods of several hours duration. The surfaces must be heated to evaporate the water over a large area or water traps must be provided to prevent refreezing of runback.

The requirement for extensive local surface heating, in addition to the aerodynamic penalties associated with inertia-separation inlets and incomplete water-droplet separation out of the air stream, will probably limit the use of these inlets as a means for turbojet-engine ice protection.

SUMMARY OF RESULTS

From an investigation of the aerodynamic and icing characteristics of several water-inertia-separation inlets of a turbojet engine, the following results were obtained:

1. Complete icing protection for inlet guide vanes of a turbojet engine could not be achieved, as evidenced by ice formations on an ice-indicator rod in the alternate duct and on ice-indicator blades at the compressor inlet.

Comparative icing rates on ice-indicator blades for a direct-ram inlet and inertia-separation inlets showed that approximately 8 percent of the volume of water available at the nacelle inlet was not separated out of the air stream by the inertia-separation inlets investigated.

2. In a nonicing condition, the total-pressure losses of the inertia-separation inlets designed to have low dynamic pressures in the main duct approached that of a conventional direct-ram inlet.

3. Total-pressure-loss values for the alternate-duct system were considerably higher than for a direct-ram inlet. It was determined that the pressure losses for the alternate-duct system were a function of duct Mach number and duct-diffuser characteristics. Severe pressure losses occurred when the duct Mach number exceeded values in the range of 0.5 to 0.6.

4. No significant effects on total-pressure losses, velocity profiles at the compressor inlet, or circumferential mass-flow shifts for the inlets investigated were observed for angles of attack up to 6°.

5. Secondary water inertia separation in the alternate duct caused heavy duct-elbow icing and resulted in a decreasing mass flow and rapid total-pressure losses, although the use of inertia-separation inlets increased the time required to reach a particular loss in pressure or mass flow by a factor of approximately 4 compared with the time required by the direct-ram inlet with compressor-inlet screen under the same conditions.

6. A mass-flow analysis of all configurations showed that only the configuration with the largest alternate-duct inlet gap (1.9 in.) could pass a mass flow through the alternate duct that is required by current engines. This air flow, however, could

only be passed through the duct at the choking Mach number with attendant high total-pressure losses. Large mass flows at Mach numbers below 1.0 at the minimum area in the alternate duct, resulting in lower total-pressure losses, may be obtained by increasing the diameter of the nacelle in order to obtain a larger alternate-duct area.

Lewis Flight Propulsion Laboratory,
National Advisory Committee for Aeronautics,
Cleveland, Ohio.

REFERENCES

1. von Glahn, Uwe: Ice Protection of Turbojet Engines by Inertia Separation of Water. I - Alternate-Duct System. NACA RM E8A27, 1948.

2. Callaghan, Edmund E., Ruggeri, Robert S., and Krebs, Richard P.: Experimental Investigation of the Hot-Gas Bleedback for Ice Protection of Turbojet Engines. I - Nacelle with Offset Air Inlet. NACA RM E8D13, 1948.

3. Naumann: Wirkungsgrad von Diffusoren bei hohen Unterschallgeschwindigkeiten. FB Nr. 1705, ZWB (Berlin-Adlershof), Dez. 18, 1942.

4. Langmuir, Irving, and Blodgett, Katherine B.: A Mathematical Investigation of Water Droplet Trajectories. Tech. Rep. No. 5418, Air Materiel Command, AAF, Feb. 19, 1946. (Contract No. W-33-038-ac-9151 with Gen. Elec. Co.)

5. Sanders, Newell D., and Behun, Michael: Generalization of Turbojet-Engine Performance in Terms of Pumping Characteristics. NACA TN 1927, 1949.

6. Acker, Loren W.: Preliminary Results of Natural Icing of an Axial-Flow Turbojet Engine. NACA RM E8C18, 1948.

TABLE I - NACELLE OUTSIDE-CONTOUR COORDINATES WITH REFERENCE TO NACELLE LEADING EDGE AND CENTER LINE

[o, outside contour; all values in inches]

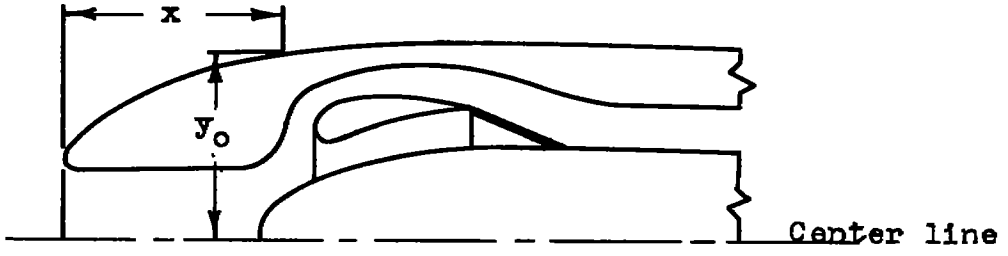

x	y_o	x	y_o	x	y_o	x	y_o
Configurations A and B; leading-edge radius, 0.375 at 6.563 above center line							
0	6.55	4.50	9.20	13.50	12.50	22.50	13.90
.188	6.82	6.00	10.40	15.00	12.75	24.00	14.00
.375	7.00	7.50	10.90	16.50	13.05	25.00	14.00
.750	7.40	9.00	11.40	18.00	13.30	26.62	14.00
1.500	7.95	10.50	11.80	19.50	13.55		
3.000	8.95	12.00	12.15	21.00	13.75		
Configurations C, D, and E; leading-edge radius, 0.375 at 7.563 above center line							
0	7.55	3.00	9.87	10.50	12.37	18.00	13.64
.188	7.87	4.50	10.50	12.00	12.70	19.50	13.80
.375	8.07	6.00	11.04	13.50	13.00	20.37	13.87
.750	8.43	7.50	11.55	15.00	13.28		
1.500	9.00	9.00	12.00	16.50	13.50		

TABLE II - NACELLE INSIDE-CONTOUR COORDINATES WITH REFERENCE TO NACELLE LEADING EDGE AND CENTER LINE

[i, inside contour; all values in inches]

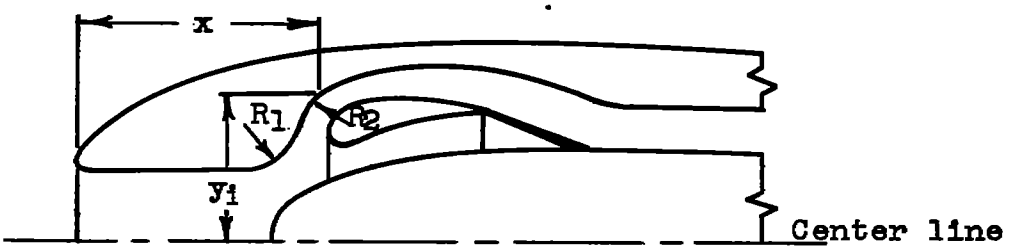

Configuration	x	y_i	Radius
B	8.187	8.375	R_1 2.50
	12.875	8.250	R_2 3.00
C, D, E	8.12	9.50	R_1 2.50
	13.10	9.00	R_2 2.50

x	y_i	x	y_i	x	y_i	x	y_i
Configuration A							
0	6.55	6.00	5.90	15.00	8.65	22.50	10.12
.188	6.20	9.00	6.00	16.50	9.05	24.00	10.30
.375	6.10	10.50	6.85	18.00	9.35	25.00	10.43
.750	6.00	12.00	7.55	19.50	9.65	26.62	10.50
3.000	5.95	13.50	8.15	21.00	9.88		
Configuration B							
0	6.55	0.375	6.10	8.18	5.88	19.00	11.38
.188	6.20	.750	6.00	13.75	11.25	26.62	10.50
Configurations C, D, and E							
0	7.55	7.00	7.00	18.50	11.37	23.12	10.94
.375	7.19	15.50	11.50	19.50	11.29	23.87	10.77
.750	7.06	16.50	11.46	20.50	11.16	24.87	10.50
1.500	7.00	17.50	11.43	21.62	10.94	25.87	10.25

TABLE III - COORDINATES FOR DUCT-SPLITTER RING AND ACCESSORY-HOUSING NOSE REFERENCED FROM RESPECTIVE NACELLE-NOSE LEADING EDGE AND NACELLE CENTER LINE

[i, inside contour and o, outside contour; all values in inches]

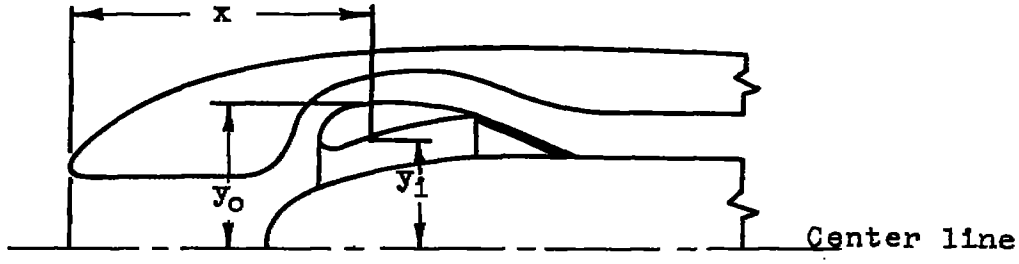

x	y_i	y_o	x	y_i	y_o	x	y_i	y_o
Configuration B; leading-edge radius, 0.600								
12.00	8.70	8.70	13.25	8.18	10.05	16.00	9.02	10.00
12.25	8.25	9.52	13.75	8.32	10.10	17.00	9.25	9.92
12.50	8.16	9.84	14.25	8.52	10.10	18.00	9.42	9.85
12.75	8.06	9.90	15.00	8.75	10.07	19.00	9.57	9.77
Configuration C; leading-edge radius, 0.600								
12.24	8.75	9.75	14.04	8.81	10.25	18.04	9.50	9.95
12.43	8.62	10.00	15.04	9.03	10.20	19.04	9.62	9.85
12.78	8.50	10.19	16.04	9.20	10.15	19.54	9.66	9.80
13.04	8.56	10.25	17.04	9.35	10.05	19.87	9.70	9.70
Configuration D; leading-edge radius, 0.600								
11.90	8.69	9.50	13.04	8.56	10.25	17.04	9.35	10.05
12.04	8.56	9.80	14.04	8.81	10.25	18.04	9.50	9.95
12.29	8.47	10.06	15.04	9.03	10.20	19.04	9.62	9.85
12.54	8.44	10.15	16.04	9.20	10.15	19.87	9.70	9.70
Configuration E; leading-edge radius, 0.600								
12.31	8.70	8.70	13.56	8.18	10.05	16.31	9.02	10.00
15.56	8.25	9.52	14.06	8.32	10.10	17.31	9.25	9.92
12.81	8.16	9.84	14.56	8.52	10.10	18.31	9.42	9.85
13.06	8.06	9.90	15.31	8.75	10.07	19.31	9.57	9.77

Accessory-housing nose coordinates							
x	y	x	y	x	y	x	y
10.000	0	12.125	3.90	15.125	5.65	18.125	6.40
10.625	2.15	13.625	4.95	16.625	6.05	19.625	6.60

A Nacelle inlet
B Accessory housing
C Radial offset, h'
D Main duct
E Main-duct static-pressure tube
F Main-duct screen
G Turning radius, R (90° angle)
H Bearing struts
I Compressor-inlet pressure rake
J Alternate-duct-inlet gap
K Duct-splitter ring
L Icing indicator, inlet guide vane
M Alternate-duct-inlet elbow
N Alternate-duct pressure rake
O Icing-indicator rod (1/16-in. diam.)
P Sheet-metal fairing (inserted for configurations C, D, and E)
Q Alternate duct

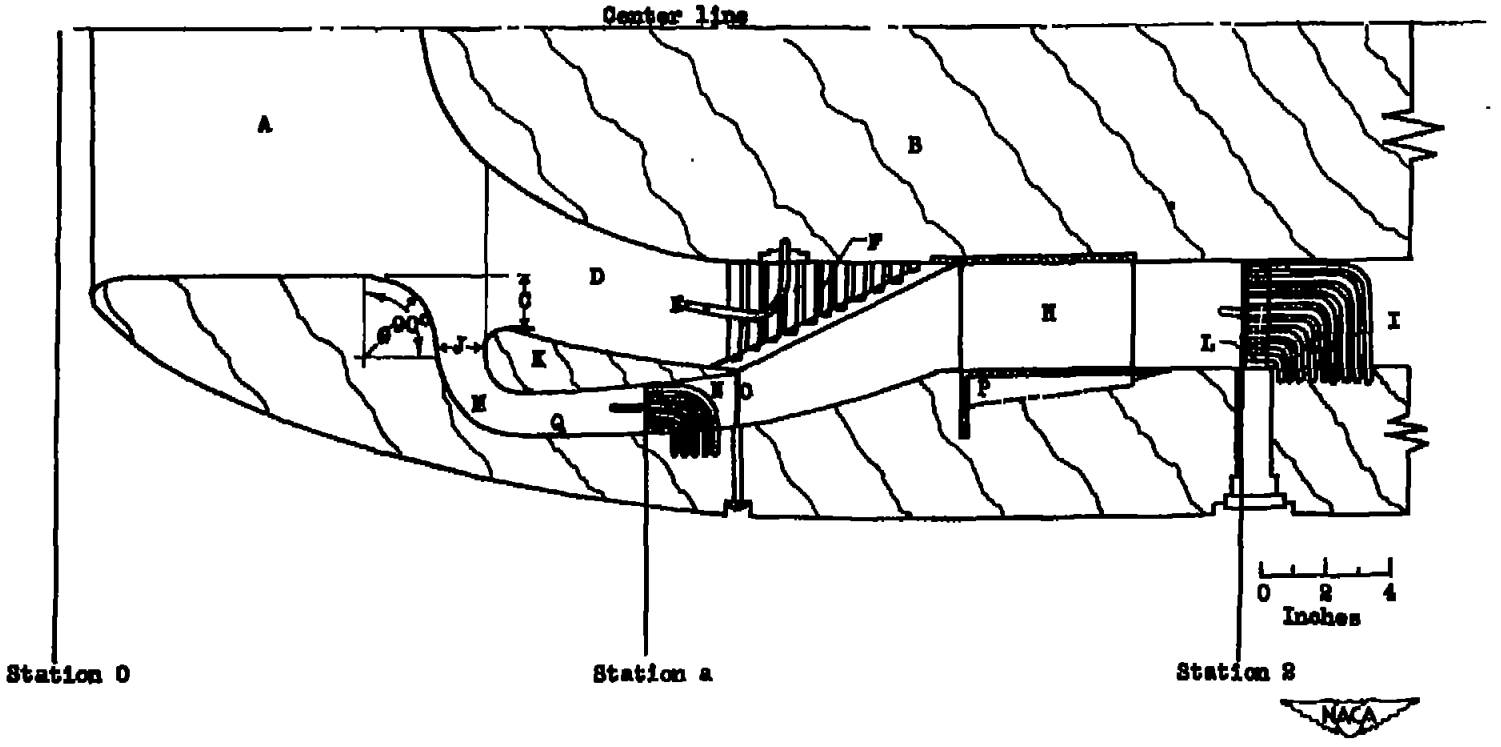

Figure 1. - Typical internal water-inertia-separation inlet showing principal components.

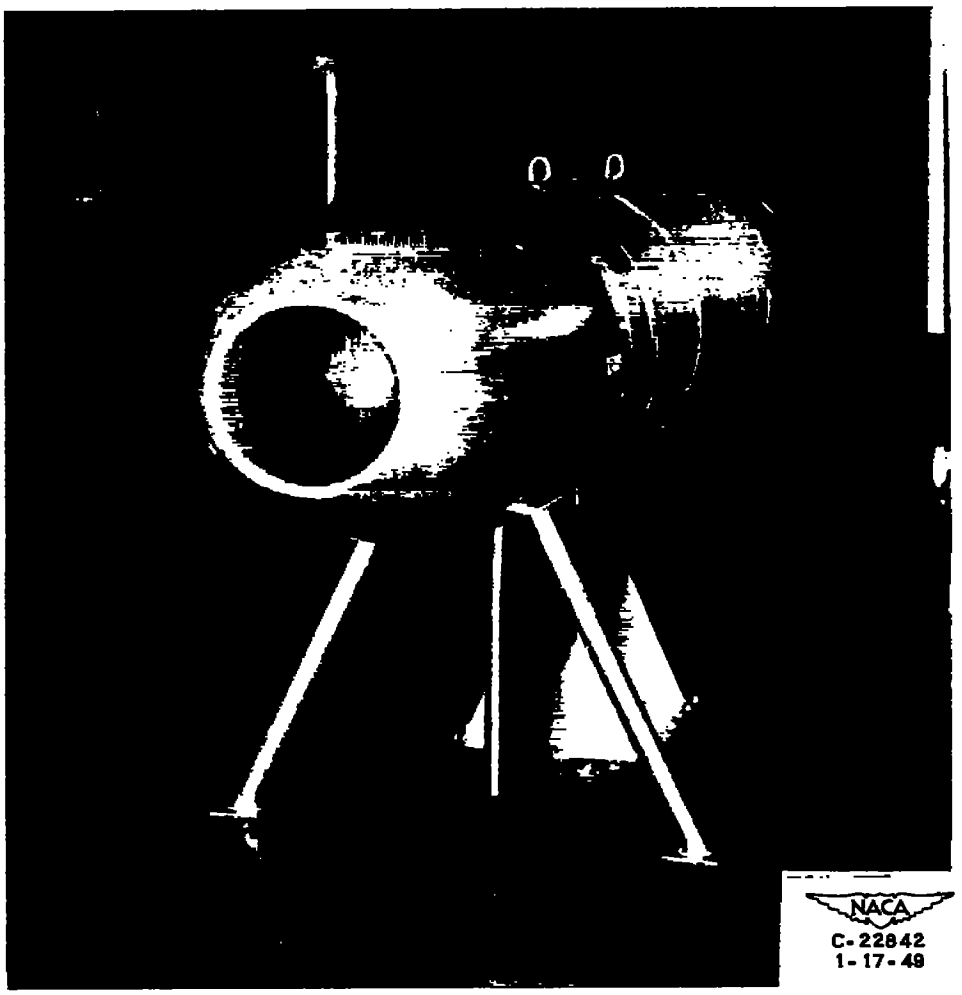

Figure 2. - Installation of typical internal water-inertia-separation nacelle inlet in icing-research tunnel.

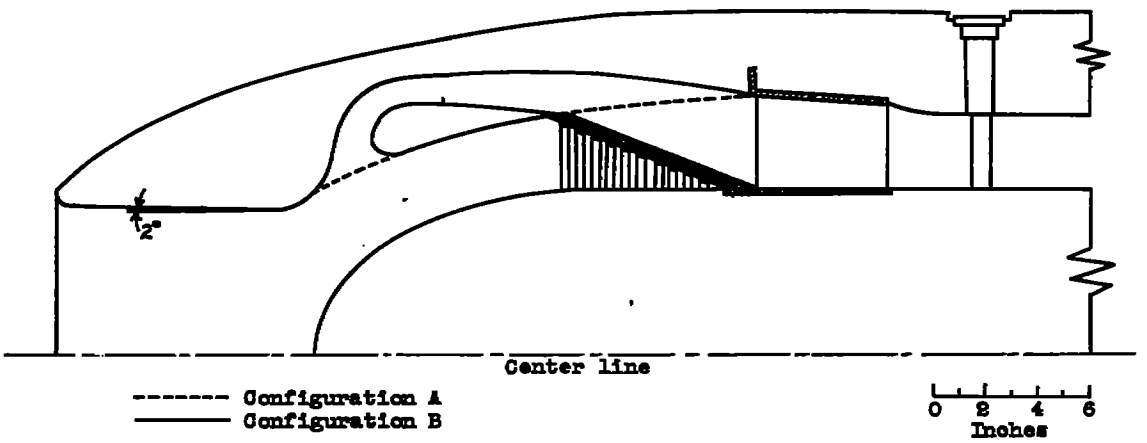

(a) High-inlet-velocity nacelle.

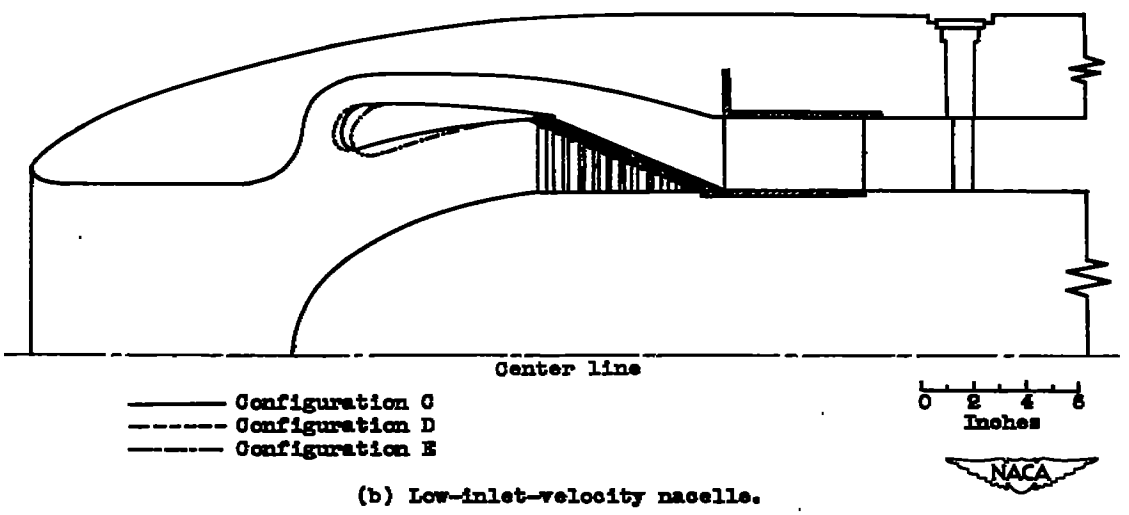

(b) Low-inlet-velocity nacelle.

Figure 3. - Cross-sectional views of nacelle configurations investigated.

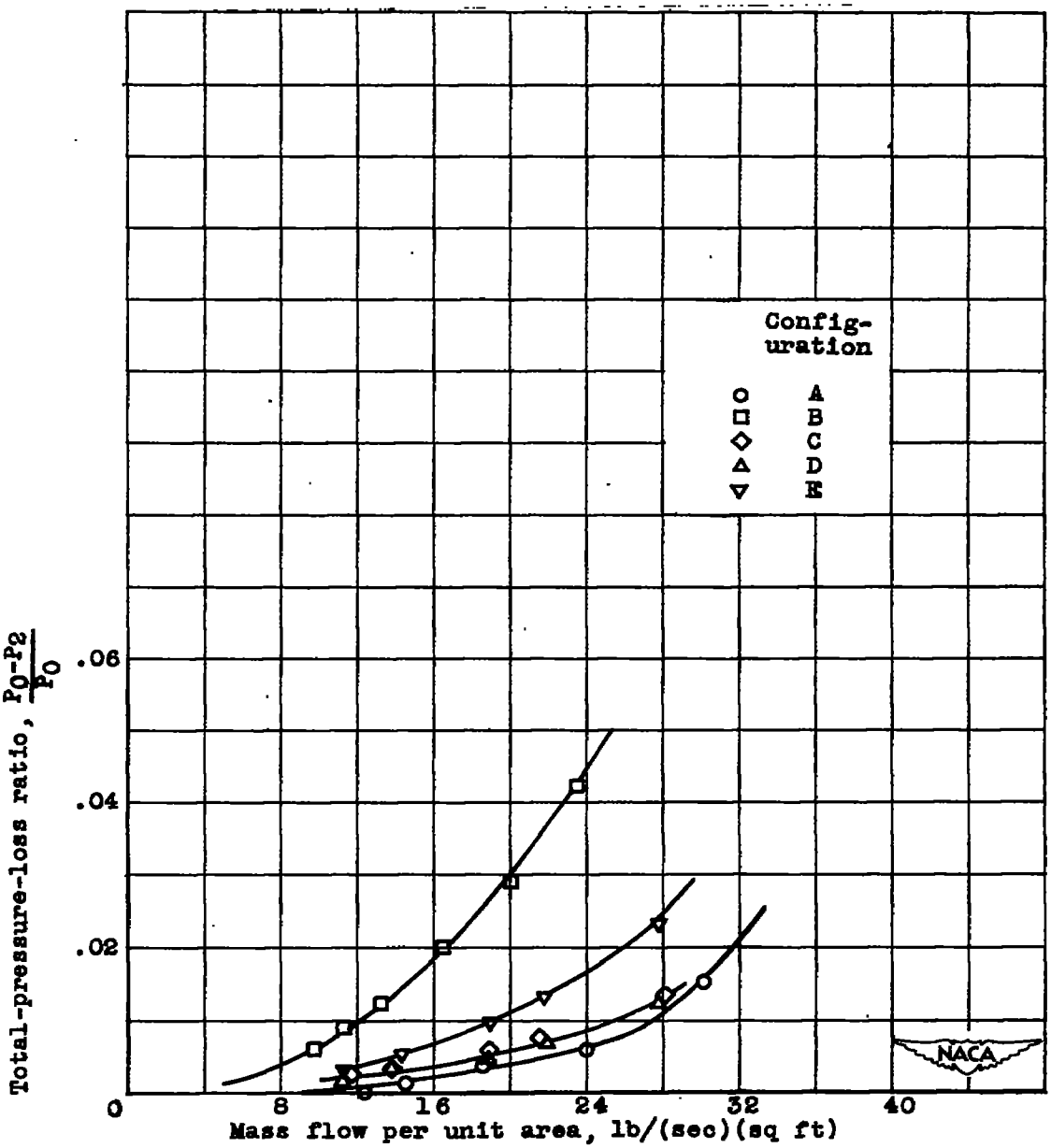

Figure 4. - Variation of over-all total-pressure-loss ratio with mass flow per unit air-flow area at compressor inlet for normal operation with main-duct screen removed. Airspeed, 250 miles per hour; angle of attack, 0°.

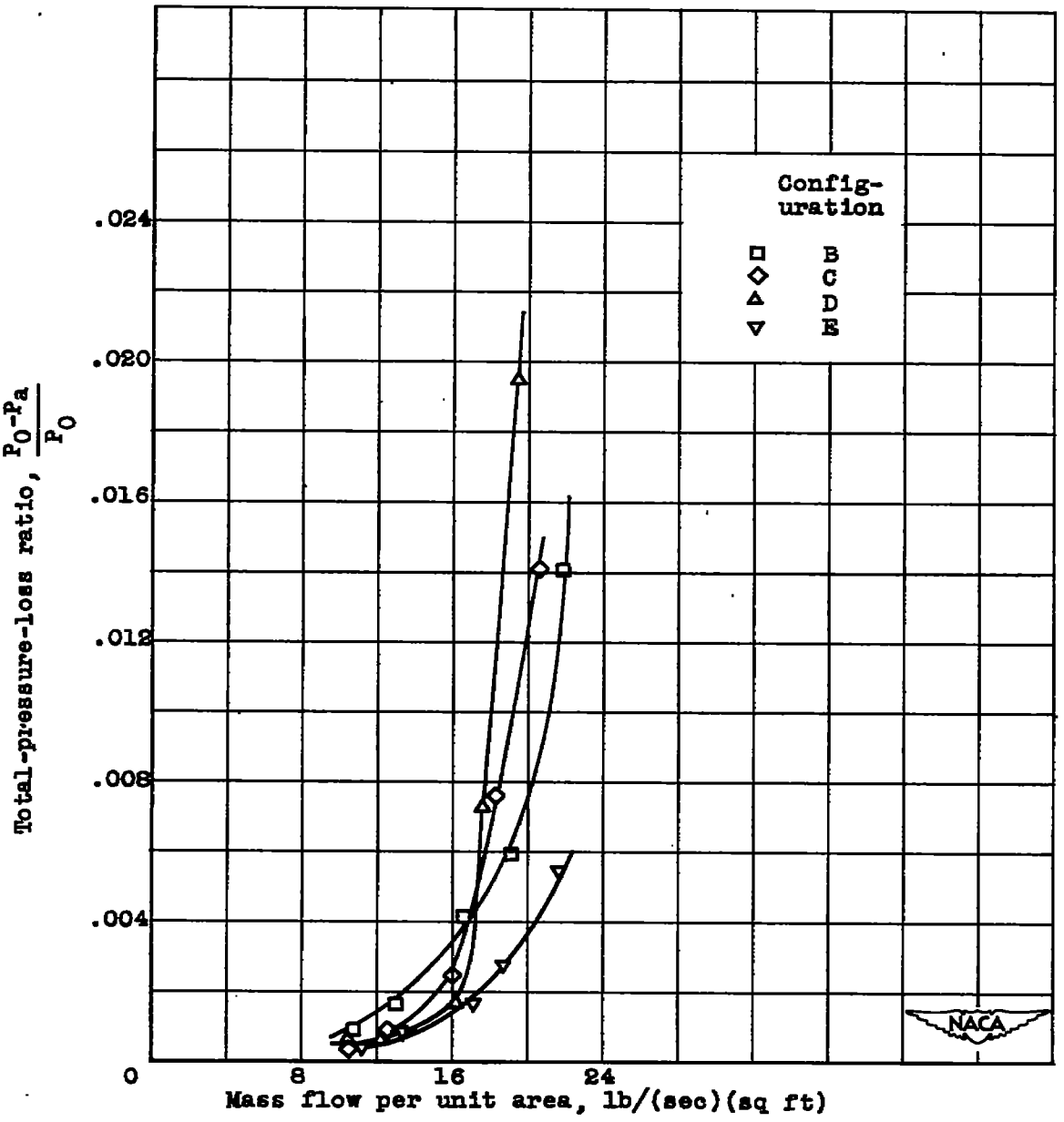

Figure 5. - Variation of total-pressure loss in alternate duct with mass flow per unit air-flow area at compressor inlet. Main duct blocked; airspeed, 250 miles per hour; angle of attack, 0°.

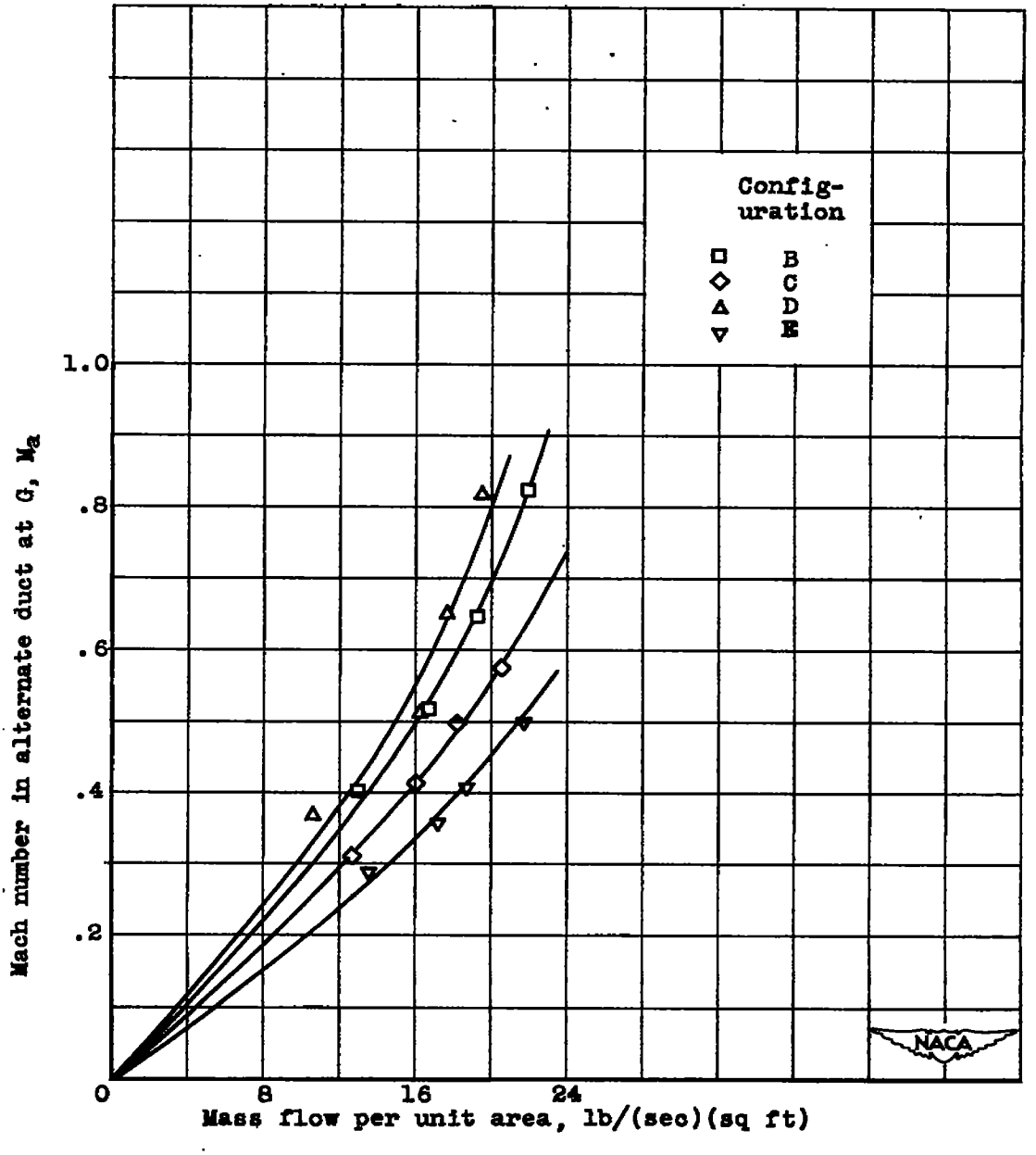

Figure 6. - Variation of alternate-duct Mach number with mass flow per unit air-flow area at compressor inlet. Main duct blocked; airspeed, 250 miles per hour; angle of attack, 0°.

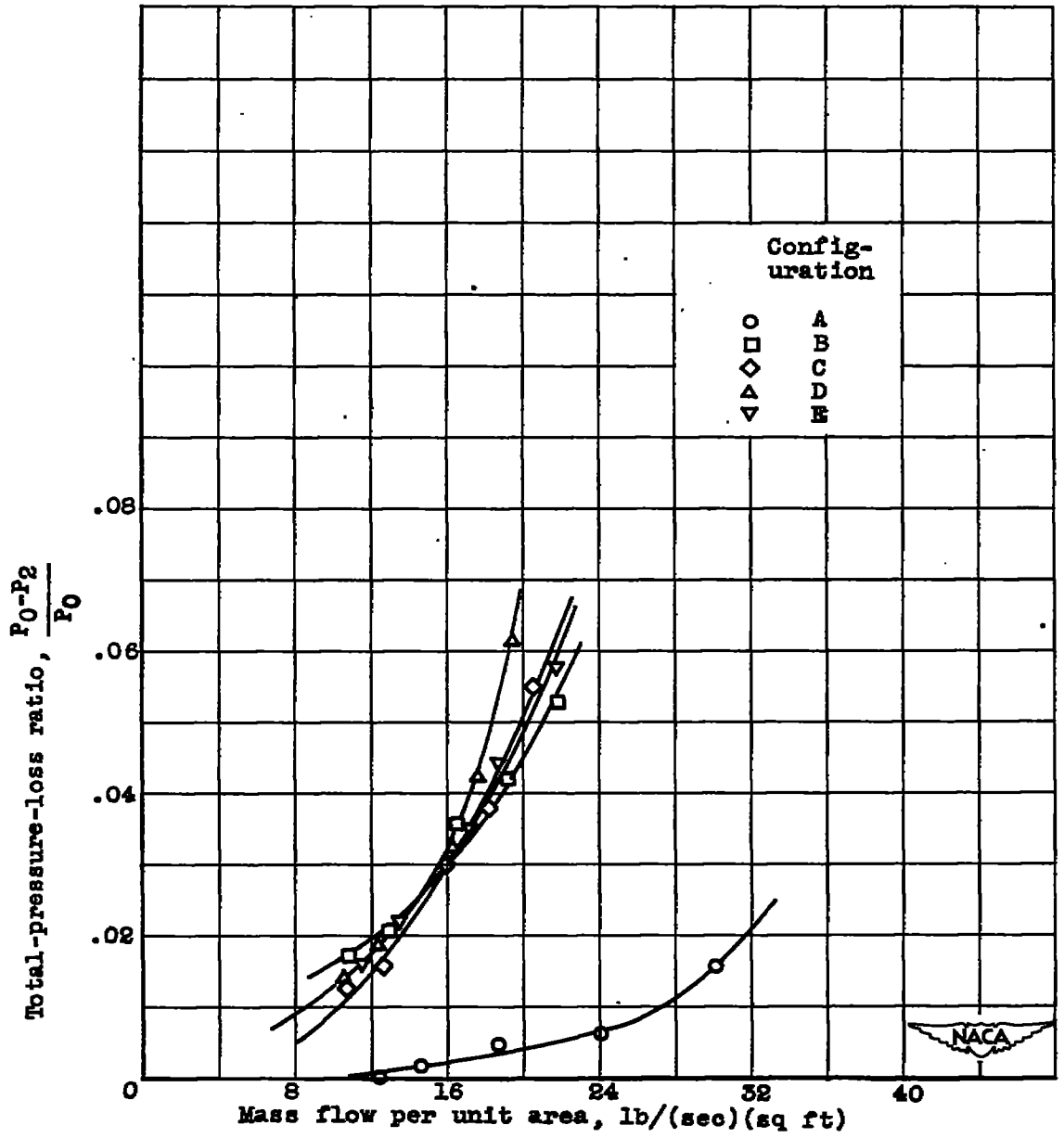

Figure 7. - Variation of over-all total-pressure-loss ratio with mass flow per unit air-flow area at compressor inlet. Main duct blocked; airspeed, 250 miles per hour; angle of attack, 0°.

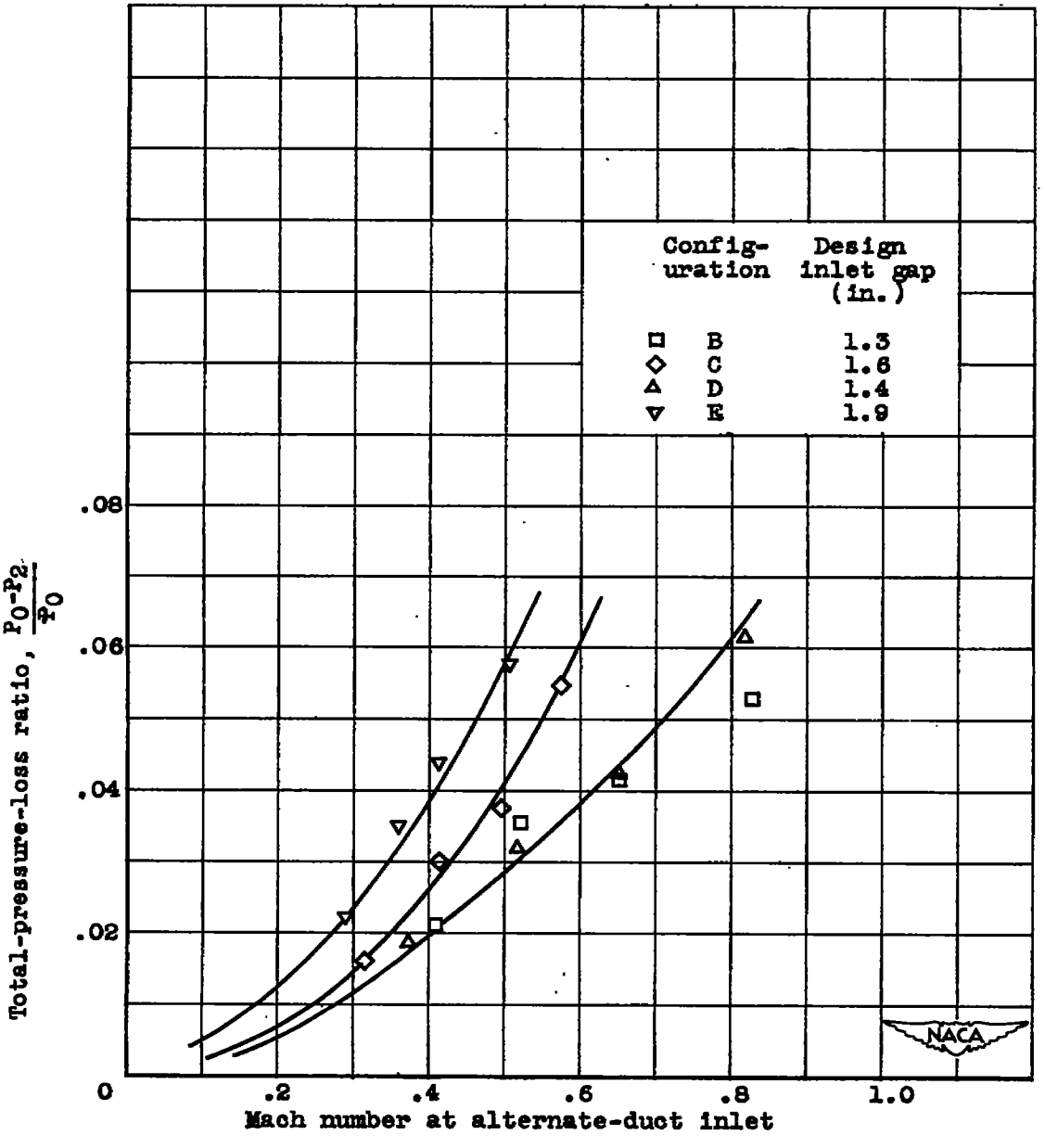

Figure 8. - Variation of total-pressure-loss ratio with Mach number at alternate-duct inlet for various inlet gaps.

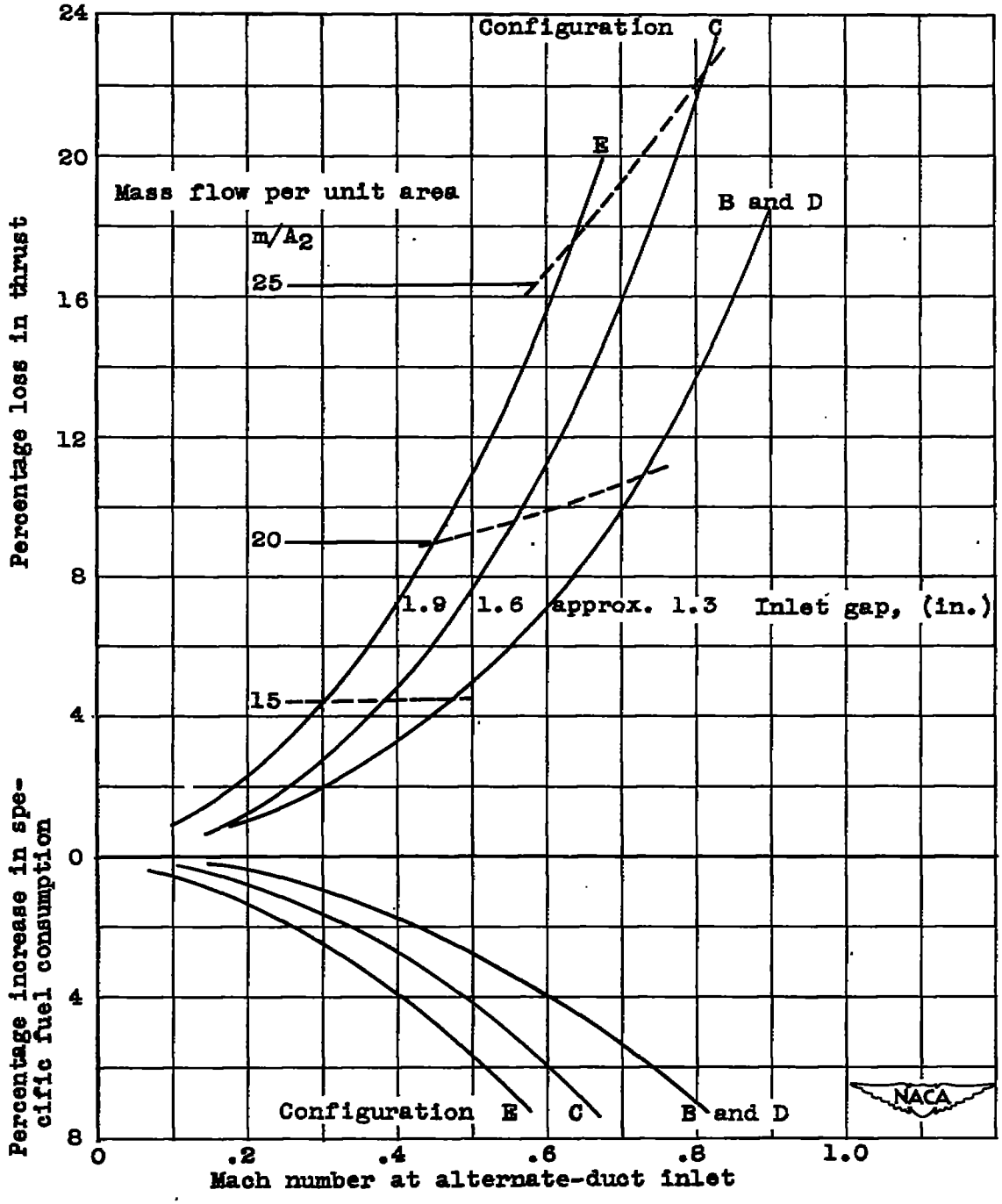

Figure 9. - Performance losses associated with inertia-separation inlets.

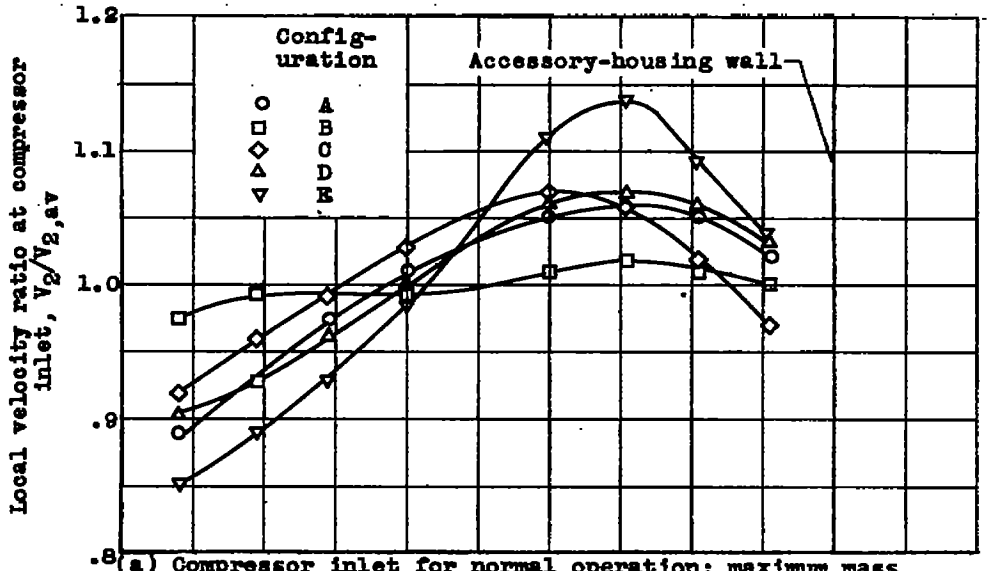

(a) Compressor inlet for normal operation; maximum mass flow per unit area, approximately 24 to 28 pounds per second per square foot.

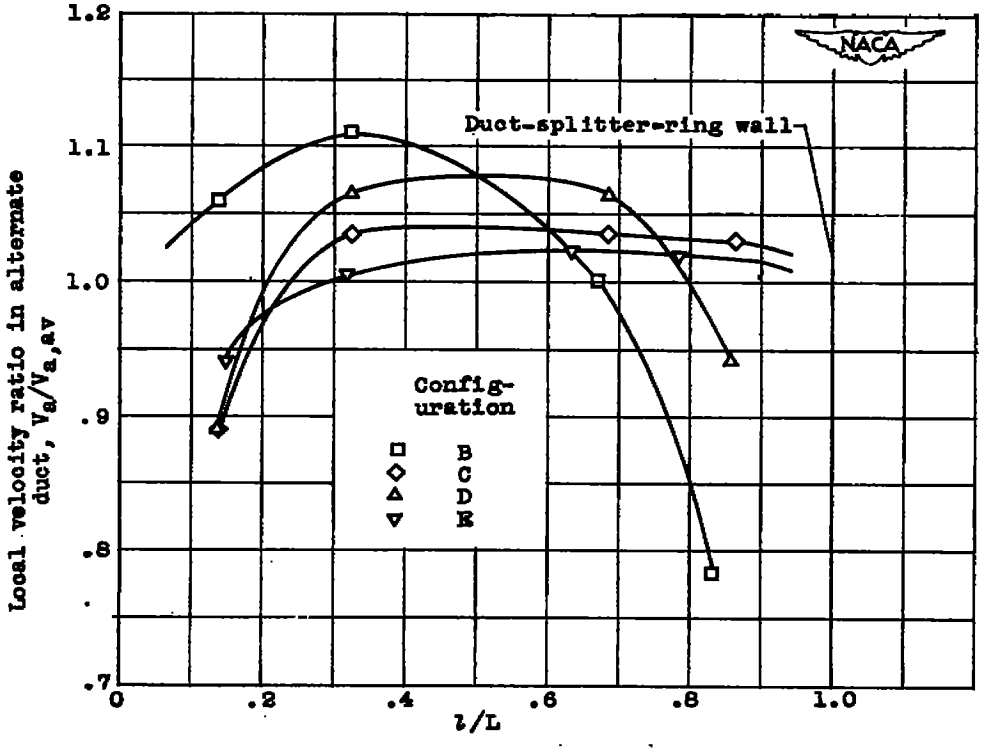

(b) Alternate duct, main duct blocked; maximum mass flow per unit area, approximately 19 to 22 pounds per second per square foot.

Figure 10. - Typical radial velocity profiles. Airspeed, 250 miles per hour; angle of attack, 0°.

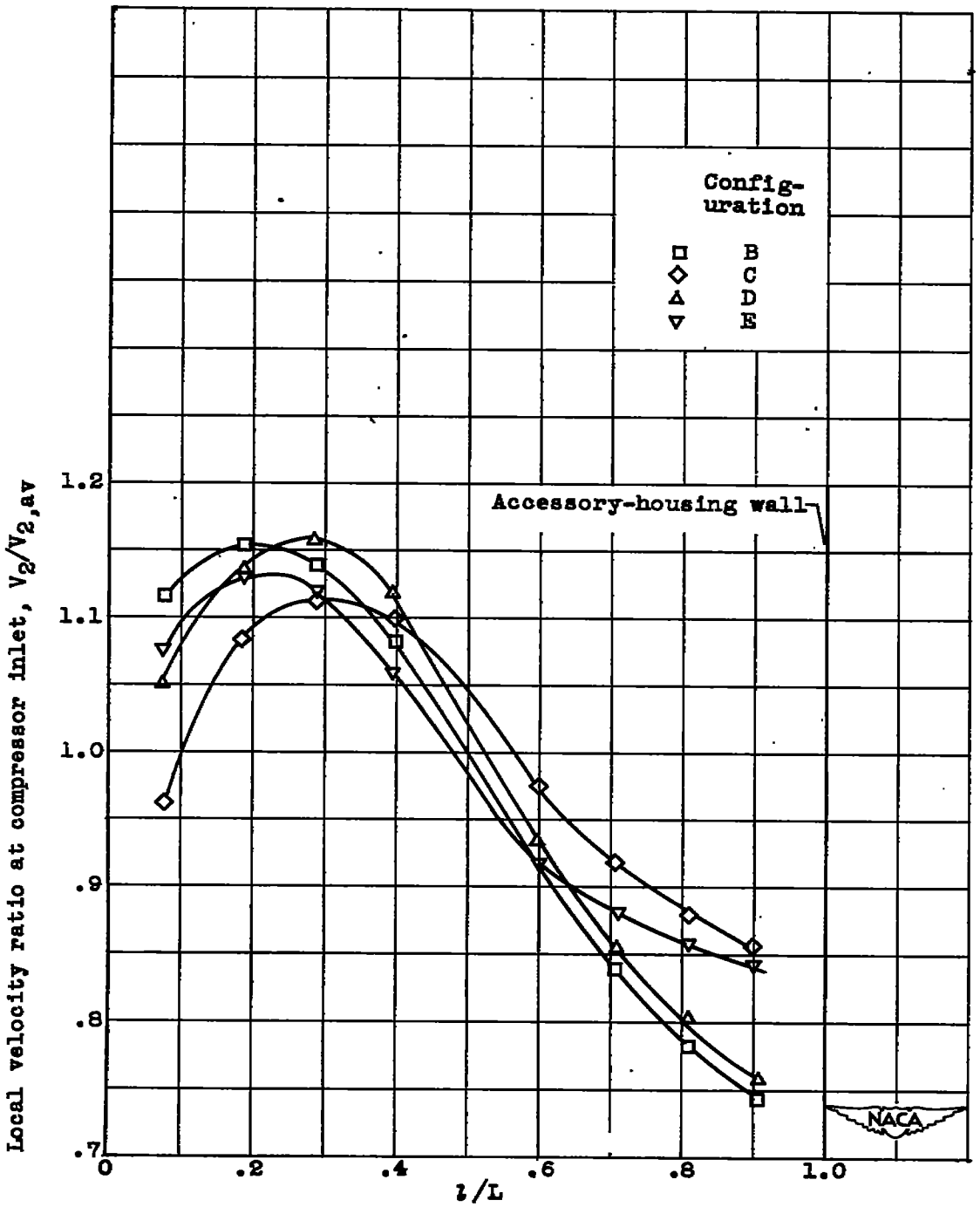

(c) Compressor inlet, main duct blocked; maximum mass flow per unit area, approximately 19 to 22 pounds per second per square foot.

Figure 10. - Concluded. Typical radial velocity profiles. Airspeed, 250 miles per hour; angle of attack, 0°.

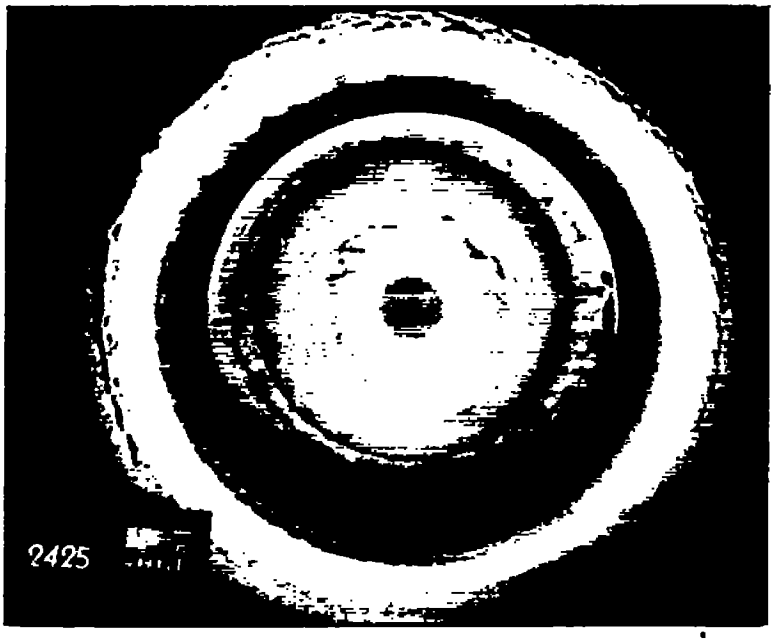

(a) Temperature, 10° F; icing period, 11 minutes; initial mass flow per unit area, 25.5 pounds per second per square foot.

(b) Temperature, 10° F; icing period, 20 minutes; initial mass flow per unit area, 12.3 pounds per second per square foot.

(c) Temperature, 20° F; icing period, 15 minutes; initial mass flow per unit area, 23.4 pounds per second per square foot.

Figure 11. - Typical ice formations on nacelle-inlet lips, nacelle-inlet walls, and accessory housing for configuration E. Airspeed, 250 miles per hour; liquid-water content, 0.6 gram per cubic meter.

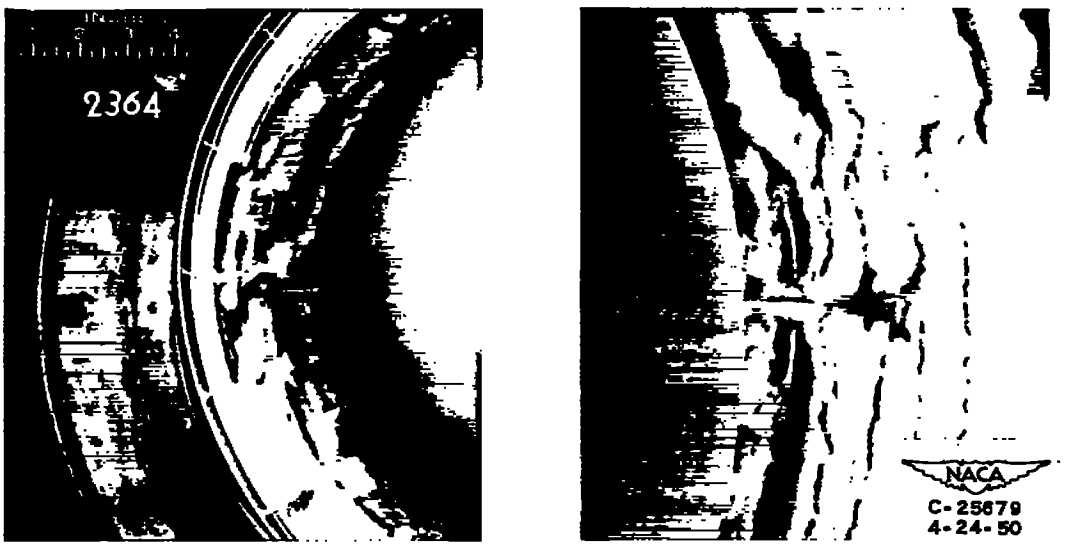

(a) Configuration A; round-wire screen; icing period, 7 minutes; initial mass flow per unit area, 21.9 pounds per second per square foot.

(b) Configuration D; streamlined-wire screen; icing period, 22 minutes; initial mass flow per unit area, 18.7 pounds per second per square foot.

Figure 12. - Typical ice formations on main-duct screen. Airspeed, 250 miles per hour; liquid-water content, 0.6 gram per cubic meter; temperature, 10° F.

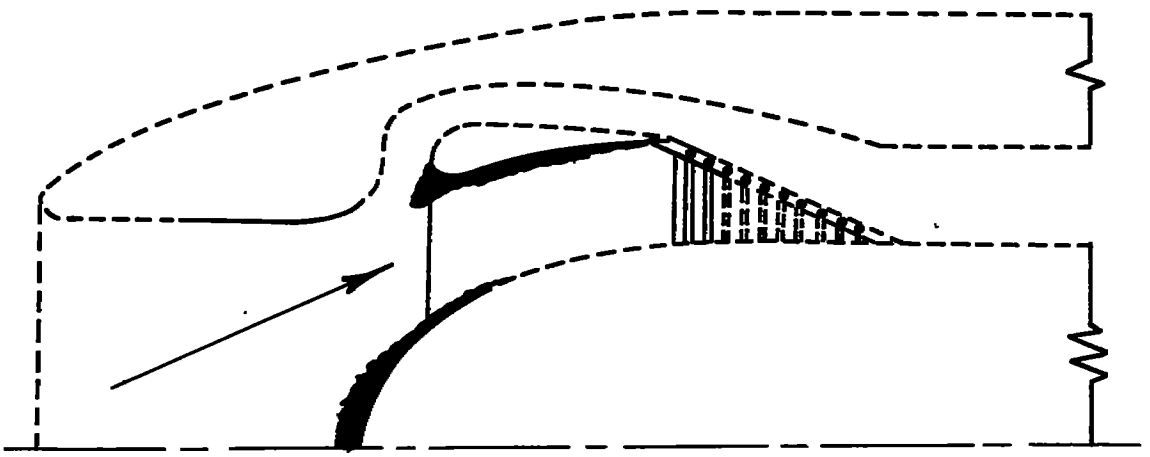

Direction of photograph

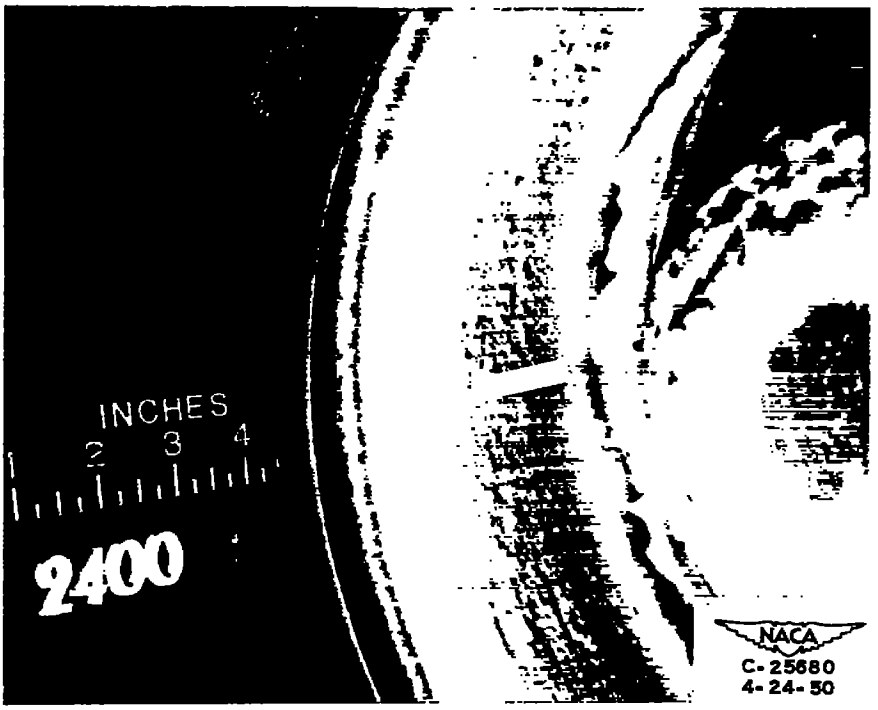

Figure 13. - Typical ice formations on duct-splitter ring of inertia-separation inlets. Round-wire screen; temperature, 10° F; airspeed, 250 miles per hour; liquid-water content, 0.6 gram per cubic meter; icing period, 11 minutes; initial mass flow per unit area, 23.7 pounds per second per square foot.

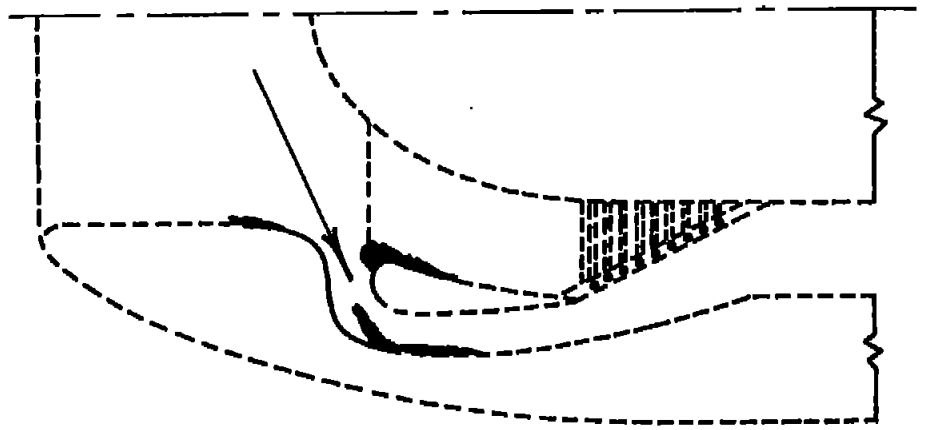

(a) Front view.

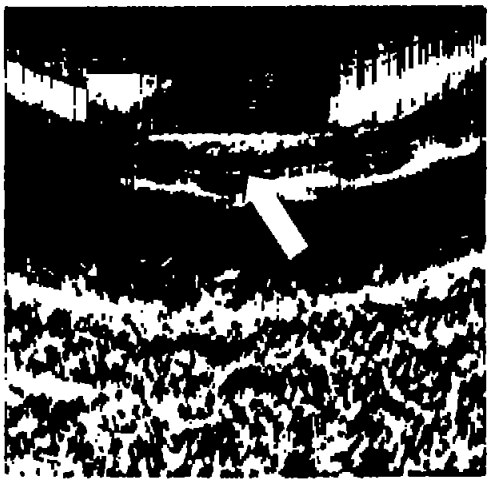

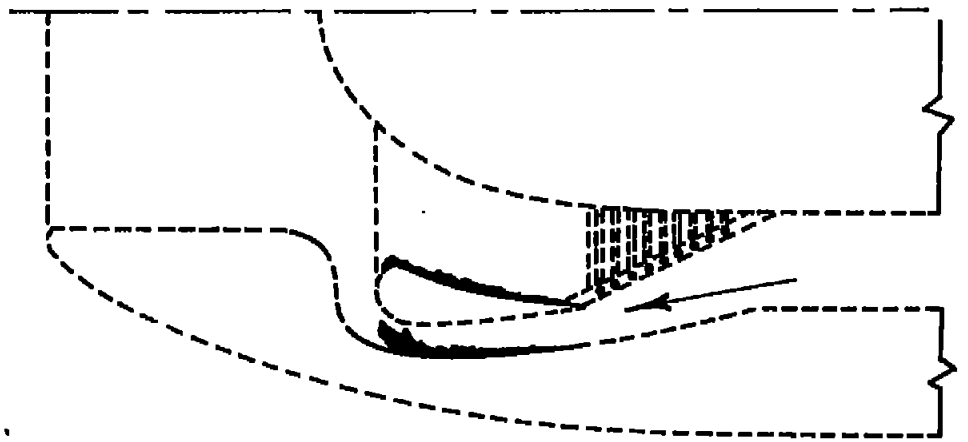

(b) Rear view.

NACA
C-25681
4-24-50

Figure 14. - Typical ice formations in alternate-duct elbow for configuration E. Airspeed, 250 miles per hour; liquid-water content, 0.8 gram per cubic meter; temperature, 10° F; icing period, 20 minutes; initial mass flow per unit area, 12.3 pounds per second per square foot.

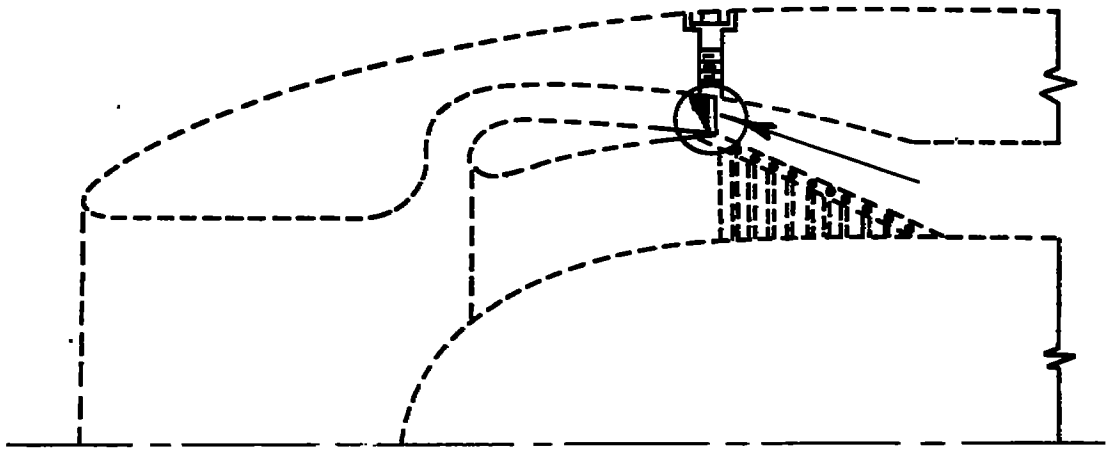

Figure 15. - Representative photograph of ice formations on 0.062-inch-diameter ice-indicator rod in alternate duct for configuration E. Airspeed, 250 miles per hour; liquid-water content, 0.6 gram per cubic meter; temperature, 10° F; icing period, 11 minutes; initial mass flow per unit area, 24.5 pounds per second per square foot.

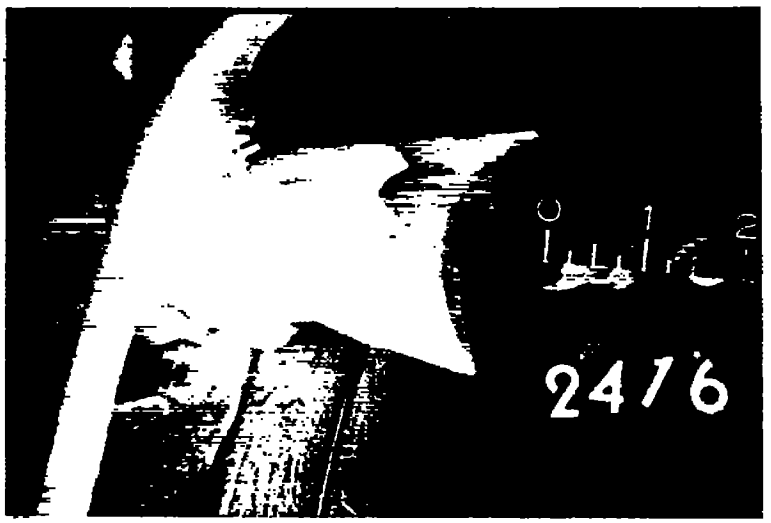

(a) Configuration A; no screen; icing period, 15 minutes; initial mass flow per unit area, 28.4 pounds per second per square foot.

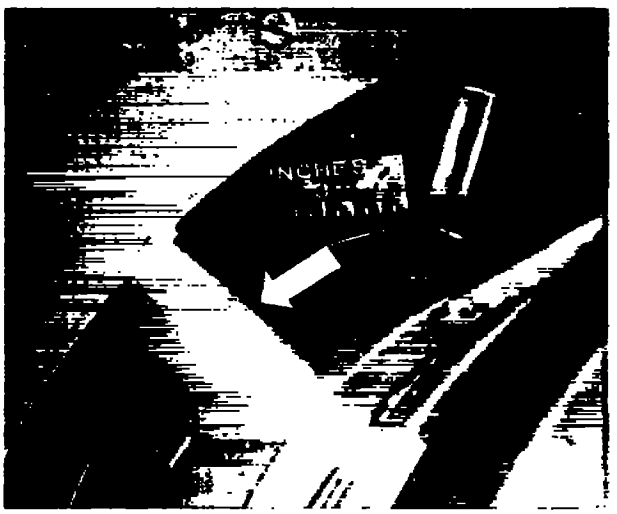

(b) Configuration C; streamlined-wire screen; icing period, 10 minutes; initial mass flow per unit area, 27.2 pounds per second per square foot.

Figure 16. - Comparison of ice formations on bearing struts for direct-ram inlet and typical inertia-separation inlet. Airspeed, 250 miles per hour; liquid-water content, 0.8 gram per cubic meter; temperature, 10° F.

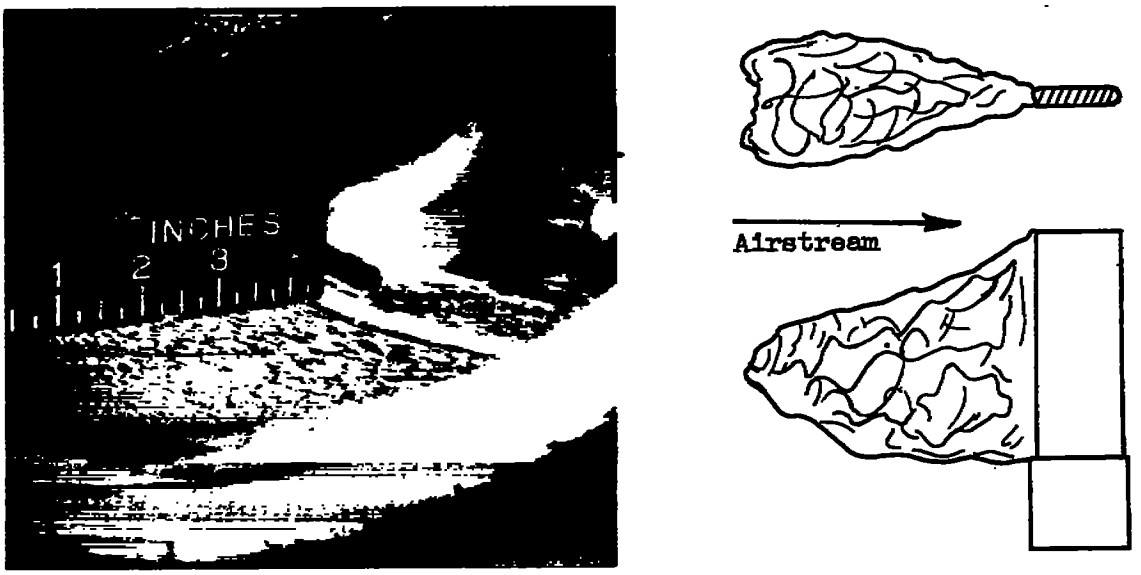

(a) Configuration A; no screen; icing period, 15 minutes; initial mass flow per unit area, 28.4 pounds per second per square foot.

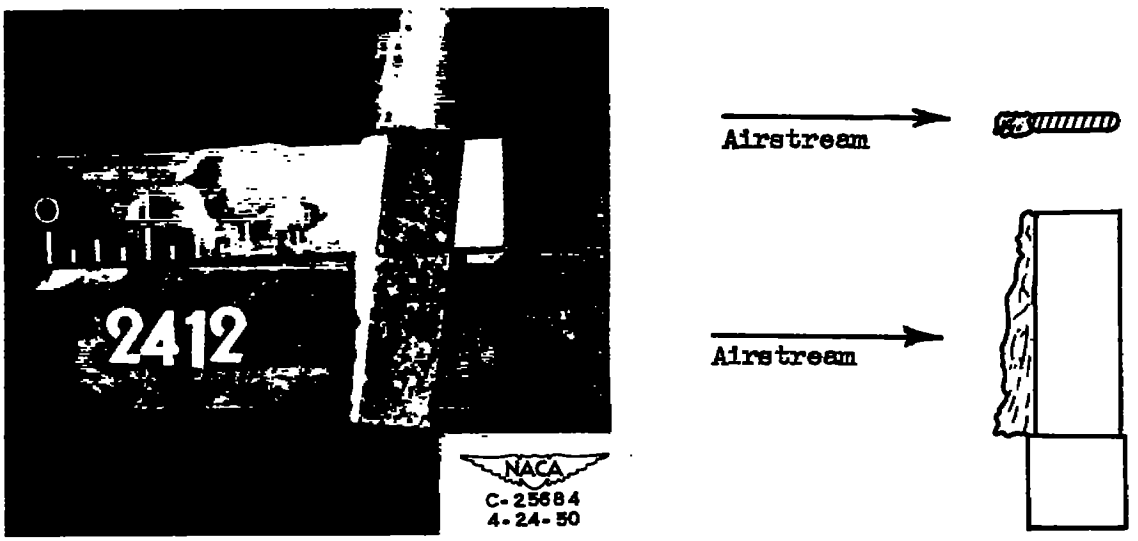

(b) Configuration E; round-wire screen; icing period, 11 minutes; initial mass flow per unit area, 24.5 pounds per second per square foot.

Figure 17. - Comparison of flat-inlet-guide-vane icing characteristics for direct-ram inlet and typical inertia-separation inlet. Airspeed, 250 miles per hour; liquid-water content, 0.6 gram per cubic meter; temperature, 10° F.

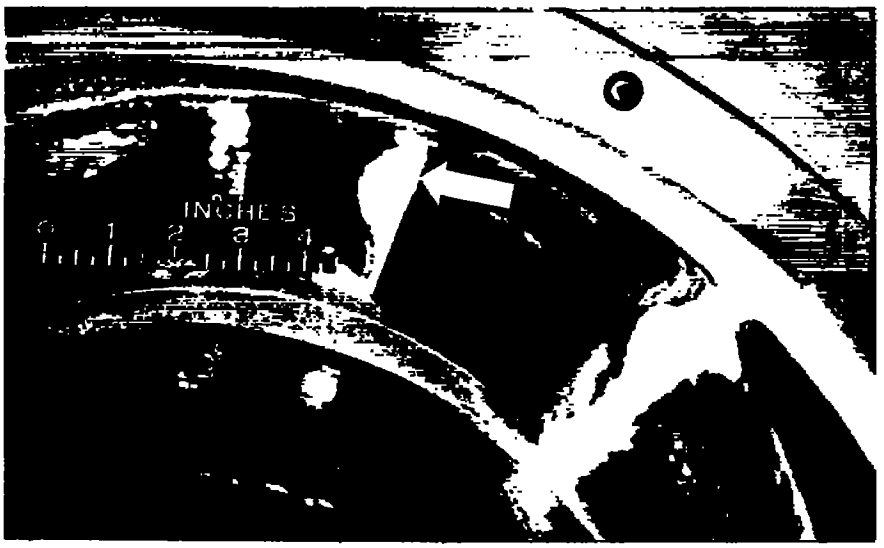

(a) Configuration A; icing period, 15 minutes; initial mass flow per unit area, 28.4 pounds per second per square foot.

(b) Configuration D; icing period, 12 minutes; initial mass flow per unit area, 17.8 pounds per second per square foot.

Figure 18. - Comparison of curved-inlet-guide-vane icing characteristics for direct-ram inlet and typical inertia-separation inlets. Airspeed, 250 miles per hour; liquid-water content, 0.6 gram per cubic meter; temperature, 10° F.

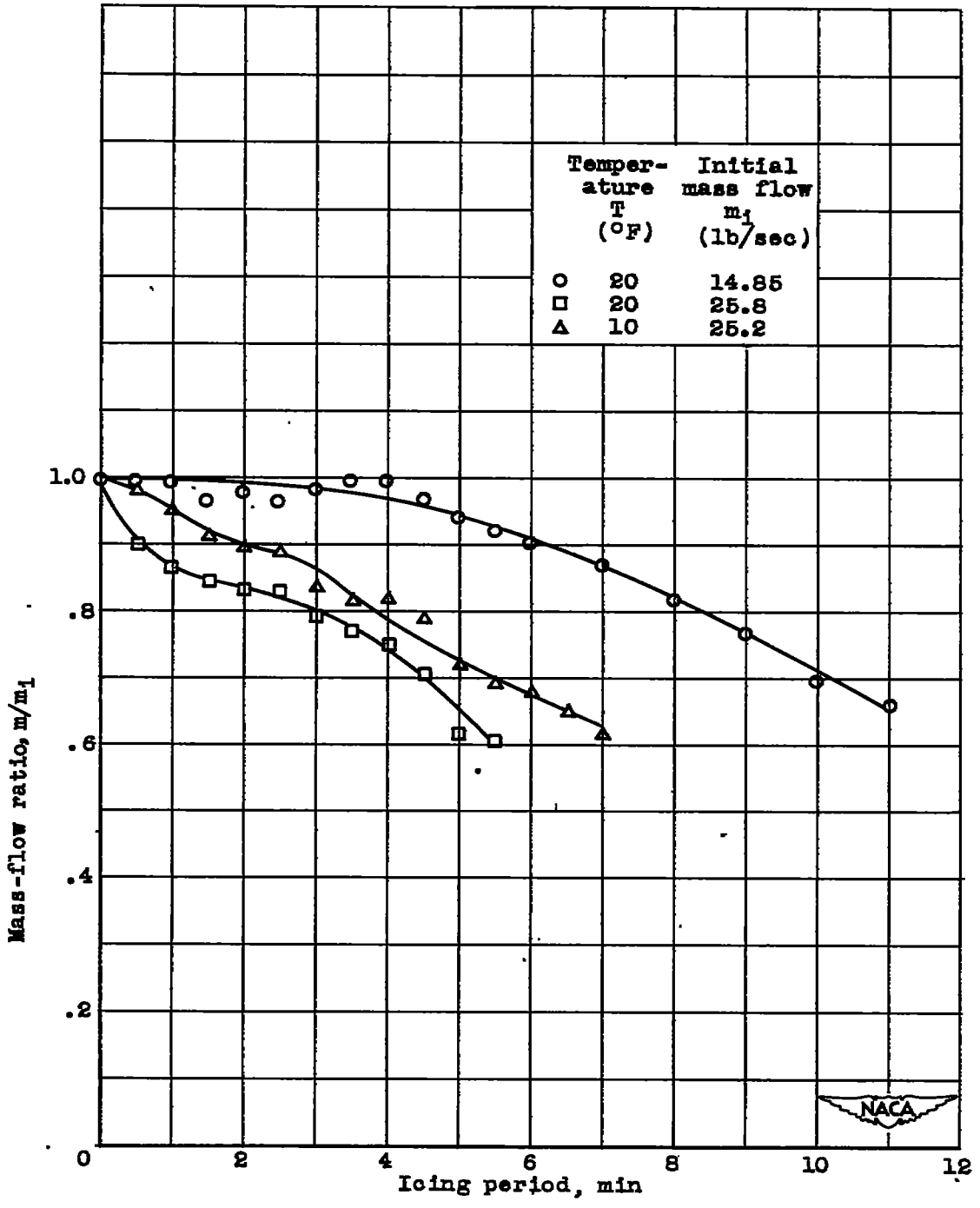

Figure 19. - Variation of mass-flow ratio for configuration A with time in icing condition. Round-wire screen; airspeed, 250 miles per hour; angle of attack, 0°; liquid-water content, 0.6 gram per cubic meter.

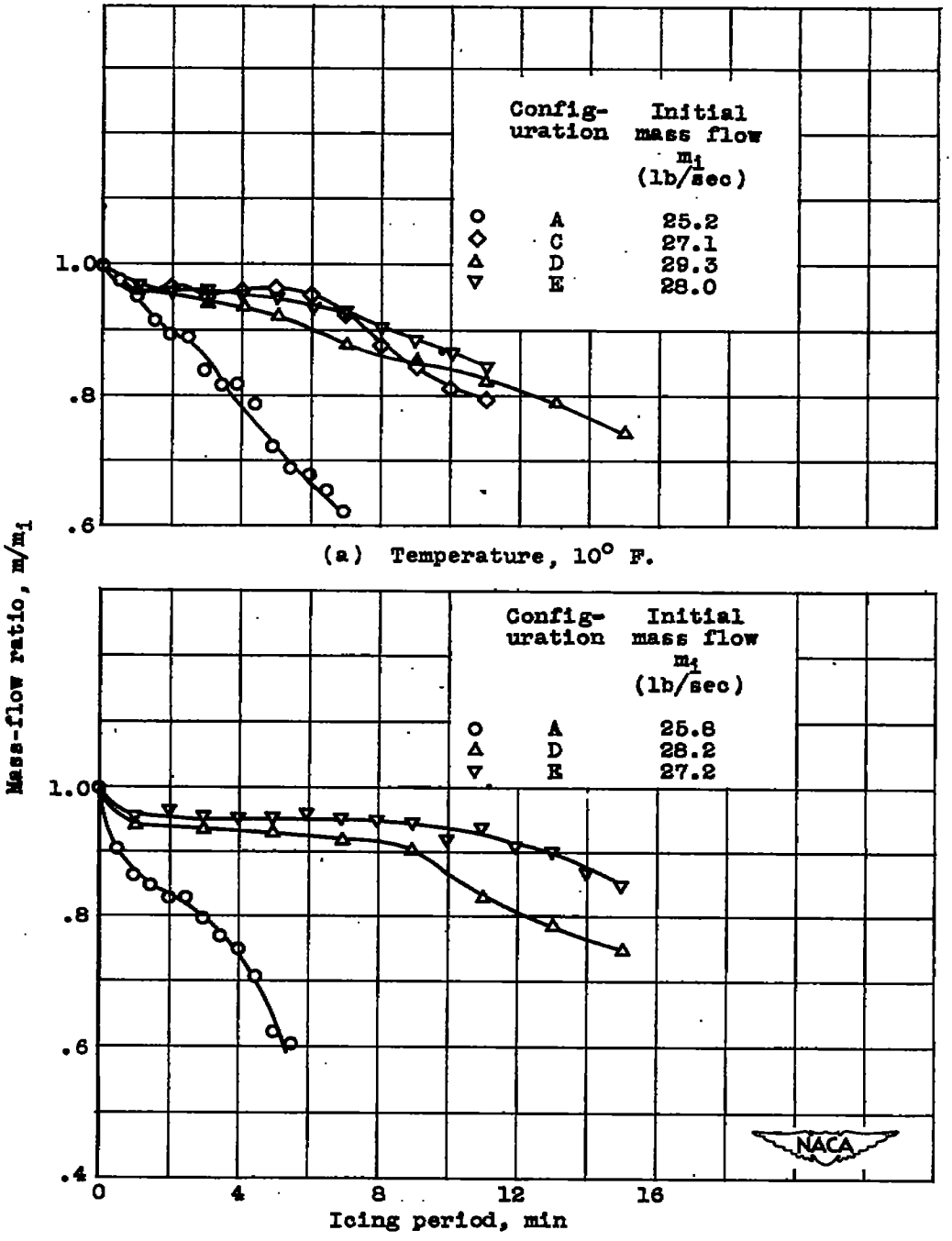

(b) Temperature, 20° F.

Figure 20. - Comparison of change in mass-flow ratio for various inlets as function of time in icing condition. Round-wire screen; airspeed, 250 miles per hour; liquid-water content, 0.6 gram per cubic meter.